

Article

Not peer-reviewed version

Mathematics of Epidemics: On the General Solution of SIRVD, SIRV, SIRD and SIR Compartment Models

[Reinhard Schlickeiser](#) * and [Martin Kröger](#) *

Posted Date: 29 February 2024

doi: 10.20944/preprints202402.1675.v1

Keywords: nonlinear differential equations; analytic solution; vaccination; pandemic spreading



Preprints.org is a free multidiscipline platform providing preprint service that is dedicated to making early versions of research outputs permanently available and citable. Preprints posted at Preprints.org appear in Web of Science, Crossref, Google Scholar, Scilit, Europe PMC.

Copyright: This is an open access article distributed under the Creative Commons Attribution License which permits unrestricted use, distribution, and reproduction in any medium, provided the original work is properly cited.

Disclaimer/Publisher's Note: The statements, opinions, and data contained in all publications are solely those of the individual author(s) and contributor(s) and not of MDPI and/or the editor(s). MDPI and/or the editor(s) disclaim responsibility for any injury to people or property resulting from any ideas, methods, instructions, or products referred to in the content.

Article

Mathematics of Epidemics: On the General Solution of SIRVD, SIRV, SIRD and SIR Compartment Models

Reinhard Schlickeiser ^{1,2,*}  and Martin Kröger ^{3,*} 

¹ Institut für Theoretische Physik, Lehrstuhl IV: Weltraum- und Astrophysik, Ruhr-Universität Bochum, D-44780 Bochum, Germany

² Institut für Theoretische Physik und Astrophysik, Christian-Albrechts-Universität zu Kiel, Leibnizstr. 15, D-24118 Kiel, Germany

³ Magnetism and Interface Physics & Computational Polymer Physics, Department of Materials, ETH Zurich, Leopold-Ruzicka-Weg 4, CH-8093 Zurich, Switzerland

* Correspondence: rsch@tp4.rub.de (R.S.); mk@mat.ethz.ch (M.K.)

Abstract: The susceptible-infected-recovered-vaccinated-deceased (SIRVD) epidemic compartment model extends the SIR model to include the effects of vaccination campaigns and time-dependent fatality rates on epidemic outbreaks. It encompasses the SIR, SIRV, SIRD, and SI models as special cases, with individual time-dependent rates governing transitions between different fractions. We investigate a special class of exact solutions and accurate analytical approximations for the SIRVD and SIRD compartment models. While the SIRVD and SIRD equations pose complex integro-differential equations for the rate of new infections and the fractions as a function of time, a simpler approach considers determining equations for the sum of ratios for given variations. This approach enables us to derive fully exact analytical solutions for the SIRVD and SIRD models. For nonlinear models with a high-dimensional parameter space, such as the SIRVD and SIRD models, analytical solutions, exact or accurately approximative, are of high importance and interest: not only as suitable benchmarks for numerical codes, but especially as they allow us to understand the critical behavior of epidemic outbursts as well as the decisive role of certain parameters. In the second part of our study, we apply a recently developed analytical approximation for the SIR and SIRV models to the more general SIRVD model. This approximation offers accurate analytical expressions for epidemic quantities, such as the rate of new infections and the fraction of infected persons, particularly when the cumulative fraction of infections is small. The distinction between recovered and deceased individuals in the SIRVD model affects the calculation of the death rate, which is proportional to the infected fraction in the SIRVD/SIRD cases but often proportional to the rate of new infections in many SIR models using a posteriori approach. We demonstrate that the temporal dependence of the infected fraction and the rate of new infections differs when considering the effects of vaccinations and when the real-time dependence of fatality and recovery rates diverge. These differences are highlighted for stationary ratios and gradually decreasing fatality rates.

Keywords: nonlinear differential equations; analytic solution; vaccination; pandemic spreading

MSC: 34A34; 34A45

Contents

1	Introduction	2
2	Compartment Models	4
2.1	SIRVD Model	4
2.2	SIRV, SIRD, SIR and SI Models	5
2.3	SIRVD Equations in Terms of the Reduced Time Variable	6
2.4	Solution of the SIRVD Equations	8

2.5	Fraction of Deceased Persons	10
3	Special Exact Solutions	10
3.1	SIRD Model	11
3.2	Constraints on the Function $\kappa(\tau)$	13
4	Details of the Construction of the SIRD Solution	15
4.1	SIRD Solution for $\kappa_\infty = 0$	16
4.2	SIRD Solution for Equal $\kappa(0) = \kappa_\infty \equiv K \neq 0$	17
4.3	Reduced time dependence of $\kappa(\tau)$, terminal time $\tau_{\text{fin}}(K)$ for $K = \kappa(0) = \kappa_\infty \neq 0$	20
4.4	Limit for Very Small Values of $I(0) = \eta \ll 1$	22
4.4.1	Case $ K - K_0 \leq \sqrt{2\eta}$	22
4.4.2	Case $ K - K_0 > \sqrt{2\eta}$	23
4.4.3	Finite Time $\tau_{\text{fin}}(K)$	23
4.4.4	Values $K < K_0 - \sqrt{2\eta}$	24
4.4.5	Values $K_0 + \sqrt{2\eta} < K \leq 2K_0$	25
4.5	SIRD Solution for $\kappa(0) = 0$	25
5	Approximate Analytical Solutions of the SIRVD Model	27
5.1	Difference between the SIRVD Death Rate and the A-Posteriori Death Rate	28
5.2	Conditions for Extrema	28
6	SIRVD Model Applications	29
6.1	Special Case: Stationary Ratios	29
6.2	Gradually Decreasing Fatality Rate	33
6.2.1	Peak Times	34
6.2.2	Maximum Rate of New Infections and Death Rate	37
6.2.3	Death Rates	37
7	Summary and Conclusions	38
A	SI Model	39
B	Integro-Differential Equation for the SIRD Model	40
C	Solution of Wright's Transcendental Equation	41
C.1	Derivation of X_0	42
C.2	Derivation of X_2	43
C.3	Derivation of X_1	43
	References	44

1. Introduction

Compartmental mathematical models are very popular and successful to describe the temporal evolution of pandemic and epidemic outbursts in populations of large size (for reviews see ref. [1–3]). Their forecasts on hospitalization and death rates help policy makers to install non-pharmaceutical interventions and/or vaccination campaigns at optimized times. As suitable compartments one introduces the fractions of susceptible persons (S), infected persons (I), recovered persons (R), deceased persons (D), and vaccinated persons (V) that no longer can be infected. Individual time-dependent rates regulate the transition between the different compartments. The temporal evolution of the epidemic is then determined by the ratios $k(t) = \mu(t)/a(t)$, $b(t) = v(t)/a(t)$ and $q(t) = \psi(t)/a(t)$ between the recovery ($\mu(t)$), vaccination ($v(t)$) and fatality ($\psi(t)$) rates to the infection ($a(t)$) rate,

respectively. By discriminating e.g. between different age classes in each compartment these models can be generalized to a much larger number of compartments in order to investigate the effects of pandemic and epidemic outbursts on persons of certain age groups. However, from the health care point of view to provide sufficiently enough intensive care beds and facilities is independent from the age of the infected persons.

Historically, the first reasonable compartment model was the susceptible–infected–recovered/removed (SIR) epidemic model [4–7]. This has been refined to include the effect of vaccination campaigns leading to the susceptible–infected–recovered/removed–vaccinated (SIRV) epidemic model [8–19]. The purpose of this manuscript is two-fold. First we will investigate new classes of exact solutions to the SIRVD and SIRD equations. Secondly we will apply the recently developed analytical approximation [20,21] for the SIR and SIRV models also to the more general SIRVD model. These accurate analytical approximations have been derived for all epidemic quantities of interest such as the rate of new infections $\dot{J}(t)$ and the corresponding cumulative fraction of infections $J(t)$. The main difference between the SIRVD and the SIRV model is the discrimination between recovered and deceased persons by introducing two different compartments. This is necessary as the omicron mutant the COVID-19 has a much smaller (about an order of magnitude) fatality rate than earlier mutants [22]. This gradually changing fatality rate is not accompanied by a corresponding change in the time dependence of the recovery rate. Therefore a mathematical description with one combined recovery/removed compartment is not sufficiently accurate anymore.

The organization of the manuscript is as follows. In Section 2, we introduce the starting dynamical equations for all considered compartment models both in terms of the real time t and the reduced time $\tau = \int_{t_0}^t d\xi a(\xi)$. It is beneficial for the analysis to express the equations in a form directly involving the observable quantities, such as the cumulative fraction of new infections $J(\tau)$ and the cumulative fraction of vaccinated persons $V(\tau)$. It is shown that for given reduced time variations of the ratios $k(\tau)$, $q(\tau)$ and $b(\tau)$ the SIRVD and SIRD equations represent complicated integro-differential equations for the rate of new infections $j(\tau)$ as well as the cumulative fraction of infections $J(\tau)$, or $S(\tau)$ and $I(\tau)$. However, the integro-differential equations can also be regarded as simpler determining equations for the sum of ratios $k(\tau) + q(\tau) = \kappa(\tau)$ for given variations of the ratio $b(\tau)$ and the fraction $S(\tau)$. This new approach is used in Section 3 to derive fully exact analytical solutions for the SIRVD and SIRD models. Especially for the SIRD model it is an effective new method to construct a special class of exact solutions depending on two parameters which are chosen as the values of the ratio $\kappa(\tau)$ at the start ($\kappa(\tau = 0)$) and the end ($\kappa(\tau = \infty)$) of the epidemic outburst. The new method for the SIRD case is illustrated in Section 4 for three different choices of the two parameters including a detailed investigation of the properties of the constructed solutions.

Sections 5 and 6 are concerned with the second main purpose of this manuscript, namely the application of the approximate analytical solution in the limit of small cumulative fractions $J \ll 1$ to the SIRVD model. For general reduced time dependencies of the ratios $k(\tau)$, $q(\tau)$ and $b(\tau)$ the time dependence of all quantities of interest is derived in Section 5, whereas in Section 6 two applications are investigated which were inaccessible to analytical treatment before. Of special interest is the calculation of the death rate $d(\tau)$ and the corresponding cumulative fraction of deceased persons $D(\tau)$. Main differences occur between the considered compartment models which reflect two alternative points of view.

In the SIRVD and SIRD case with a prescribed fatality rate $\psi(t)$, corresponding to the ratio $q(\tau)$, the death rate is proportional to the fraction $I(t)$. Moreover, any different reduced time dependencies of the ratios $k(\tau)$ and $q(\tau)$ correctly enter the dynamical equations. In contrast, in the SIR models no compartment of deceased persons has been considered. Instead the total fraction of recovered and removed (by death) populations $R_{\text{tot}}(t)$ and the summed recovery/removed rate $\mu_{\text{tot}}(t)$ are used. Then the solution for the rate of new infections $\dot{J}_{\text{SIR}}(t)$ is employed to calculate an *a posteriori* death rate as [6] $d_{\text{a-pos}} = \psi(t)\dot{J}_{\text{SIR}}(t)$ from a specified fatality rate $\psi(t)$. Of course, this fatality rate can be regarded as part of the summed recovery/removed rate, so that it also enters the dynamical SIR

model equations. However, the main difference remains for the calculation of the death rate: in the SIRVD/SIRD cases it is proportional to $I(t)$, whereas in many SIR models it is proportional to $\dot{I}(t)$. And the temporal dependence of $I(t)$ and $\dot{I}(t)$ can be different. As we will show the disparity is most pronounced when the effect of vaccinations is included and/or when the real time dependence of the fatality rate $\psi(t)$ and the recovery rate $\mu(t)$ are different from each other. The a-posteriori approach not necessarily is incorrect but has his own justification. It assumes that the probability to die from the virus infection is only determined by being or having been infected with it, and thus is proportional to the rate of new infections $\dot{I}(t)$. In contrast in the SIRD and SIRVD models the probability to die is the same on every day being infected and thus depends on the duration of the infection. A summary and conclusion (Section 7) completes the manuscript.

2. Compartment Models

2.1. SIRVD Model

We start with the SIRVD epidemics model described by four transition rates regulating the transitions between the five compartments: the fractions of susceptible persons (S), infected persons (I), recovered persons (R), removed by death persons (D), and vaccinated persons (V) that no longer can be infected. The transition rates in general are time-dependent and different from each other. The infection rate $a(t)$ regulates the transition from $S \rightarrow I$, the vaccination rate $v(t)$ the transition $S \rightarrow V$, the fatality rate $\psi(t)$ the transition $I \rightarrow D$, and the recovery rate $\mu(t)$ the transition $I \rightarrow R$, respectively (Figure 1). The SIRVD equations read:

$$\dot{S} = -a(t)SI - v(t)S, \quad (1a)$$

$$\dot{I} = a(t)SI - \mu(t)I - \psi(t)I, \quad (1b)$$

$$\dot{R} = \mu(t)I, \quad (1c)$$

$$\dot{D} = \psi(t)I, \quad (1d)$$

$$\dot{V} = v(t)S, \quad (1e)$$

where the dot stands for a derivative with respect to time t . The five fractions obey the sum constraint

$$S(t) + I(t) + R(t) + D(t) + V(t) = 1 \quad (2)$$

at all times $t \geq t_0$ after the start of the wave at time t_0 with the initial conditions of the so-called semi-time case

$$I(t_0) = \eta, \quad S(t_0) = 1 - \eta, \quad R(t_0) = 0, \quad D(t_0) = 0, \quad V(t_0) = 0, \quad (3)$$

where η is positive and usually very small, $\eta \ll 1$.

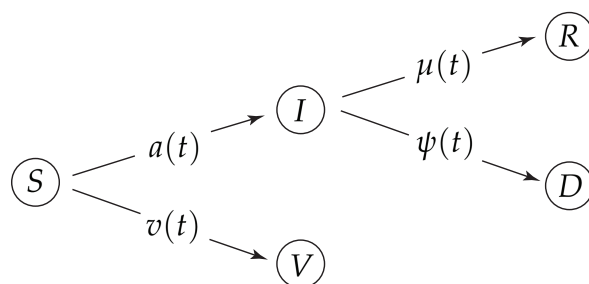


Figure 1. The dynamical SIRVD model captures transitions between five compartments by four dimensional rates as shown. Using the dimensionless time τ defined in Equation (9), one is left with three dimensionless rates $k(\tau)$, $b(\tau)$, and $q(\tau)$, c.f., Equation (10), leading to the dimensionless form of the SIRVD model, Equations (11a)–(11f).

2.2. SIRV, SIRD, SIR and SI Models

The SIRVD model includes as special cases the SIRV, SIRD and SIR epidemics models. For these three simpler models one introduces the total fraction of recovered and removed (by death) populations

$$R_{\text{tot}}(t) = R(t) + D(t), \quad (4)$$

and the summed recovery/removed rate

$$\mu_{\text{tot}}(t) = \mu(t) + \psi(t). \quad (5)$$

By this modification the five individual compartments of the SIRVD models are reduced to four compartments in the SIRV-description and to three compartments in the SIR-description, respectively. Consequently, the SIRVD Equations (1a)–(2) become

$$\dot{S} = -a(t)SI - v(t)S, \quad (6a)$$

$$\dot{I} = a(t)SI - \mu_{\text{tot}}(t)I, \quad (6b)$$

$$\dot{R}_{\text{tot}} = \mu_{\text{tot}}(t)I, \quad (6c)$$

$$\dot{V} = v(t)S, \quad (6d)$$

$$S(t) + I(t) + R_{\text{tot}}(t) + V(t) = 1, \quad (6e)$$

which apart from a slight change in notation (R_{tot} and μ_{tot} instead of R and μ before) agree exactly with the earlier considered Equations (13) - (17) in [21].

The SIRD and SIR models ignore the effect of vaccinations so that $v(t) = V(t) = 0$. The time evolution in the SIRD model is then given by taking the limit $v(t) = V(t) = 0$ of the Equations (1)–(2) yielding

$$\dot{S} = -a(t)SI, \quad (7a)$$

$$\dot{I} = a(t)SI - \mu(t)I - \psi(t)I, \quad (7b)$$

$$\dot{R} = \mu(t)I, \quad (7c)$$

$$\dot{D} = \psi(t)I, \quad (7d)$$

$$S(t) + I(t) + R(t) + D(t) + V(t) = 1. \quad (7e)$$

Likewise, the limit $v(t) = V(t) = 0$ of the Equations (6) provide the SIR equations for the three remaining compartments:

$$\dot{S} = -a(t)SI - v(t)S, \quad (8a)$$

$$\dot{I} = a(t)SI - \mu_{\text{tot}}(t)I, \quad (8b)$$

$$\dot{R}_{\text{tot}} = \mu_{\text{tot}}(t)I, \quad (8c)$$

$$S(t) + I(t) + R_{\text{tot}}(t) = 1 \quad (8d)$$

For completeness we discuss the SI model where additionally $\mu(t) = 0$ in Appendix A.

2.3. SIRVD Equations in Terms of the Reduced Time Variable

It is convenient to introduce the reduced time [6]

$$\tau = \int_{t_0}^t d\zeta a(\zeta), \quad (9)$$

and the dimensionless ratios

$$k(\tau) = \frac{\mu(\tau(t))}{a(\tau(t))}, \quad b(\tau) = \frac{v(\tau(t))}{a(\tau(t))}, \quad q(\tau) = \frac{\psi(\tau(t))}{a(\tau(t))}. \quad (10)$$

Then the SIRVD Equations (1a)–(2) can be written as

$$\frac{dS}{d\tau} = -SI - b(\tau)S, \quad (11a)$$

$$\frac{dI}{d\tau} = SI - [k(\tau) + q(\tau)]I, \quad (11b)$$

$$\frac{dR}{d\tau} = k(\tau)I, \quad (11c)$$

$$\frac{dD}{d\tau} = q(\tau)I, \quad (11d)$$

$$\frac{dV}{d\tau} = b(\tau)S, \quad (11e)$$

$$S(\tau) + I(\tau) + R(\tau) + D(\tau) + V(\tau) = 1. \quad (11f)$$

subject to initial conditions $I(0) = \eta = 1 - S(0)$ and $R(0) = D(0) = V(0) = 0$.

By solving Equations (11) numerically for the case of stationary ratios $k(\tau) = 0.5$, $b(\tau) = 0.01$, $q(\tau) = 0.1$, one establishes quantitatively different temporal dependencies for the various fractions of the four different models SIR, SIRD, SIRV and SIRVD (see Figure 2). Numerical schemes have been developed especially for the SIR model, see the recent works [14,23,24]. We used a variable-step, variable-order (VSVO) Adams-Bashforth-Moulton PECE solver of orders 1 to 13 to produce Figure 2. The highest order used appears to be 12, however, a formula of order 13 is used to form the error estimate and the function does local extrapolation to advance the integration at order 13 [25]. This Figure is meant as a motivation for the following analysis which has the aim to understand the different behaviors of the four models on the basis of analytical calculations. Our analytical study also will be concerned with in general time dependent ratios $k(\tau)$, $q(\tau)$ and $b(\tau)$. Moreover, it will derive new methods to construct special classes of exact analytical solutions.

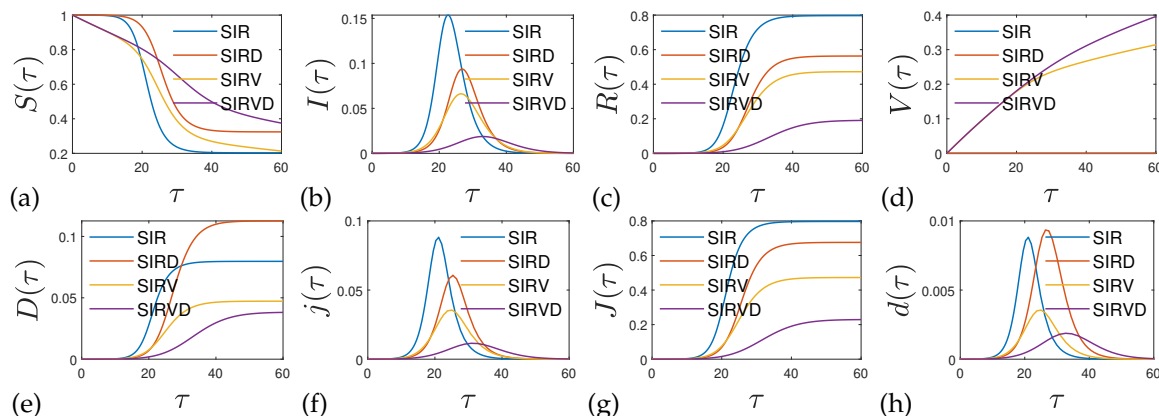


Figure 2. Quantitative comparison between the four models at identical, constant rates, $k(\tau) = 0.5$, $b(\tau) = 0.01$, $q(\tau) = 0.1$, and $\eta = 10^{-5}$. Shown are numerical solutions for (a) susceptible fraction $S(\tau)$, (b) infected fraction $I(\tau)$, (c) recovered fraction $R(\tau)$, (d) vaccinated fraction $V(\tau)$, (e) deceased fraction $D(\tau)$, (f) newly infected fraction $j(\tau) = S(\tau)I(\tau) = dJ(\tau)/d\tau$, (g) cumulative infected fraction $J(\tau) = 1 - S(\tau) - V(\tau)$, (h) newly deceased fraction $d(\tau) = dD(\tau)/d\tau$.

To this end it turns out important to introduce the rate of new infections, $\dot{J}(t) = a(t)S(t)I(t)$, that determines in the absence of vaccination the reduction of the susceptible compartment according to Equation (1a). Its dimensionless counterpart, appearing in Equation (11a), is

$$j(\tau) = S(\tau)I(\tau) = \frac{dJ(\tau)}{d\tau}, \quad (12)$$

so that $\dot{J}(t) = a(t)j(\tau)$ and $j(\tau = 0) = \eta(1 - \eta)$. In terms of the rate of new infections $j(\tau)$, and the corresponding cumulative fraction of new infections

$$J(t) = J(\tau) = \eta + \int_0^\tau dx j(x), \quad (13)$$

Equations (11a) and (11e)–(11f) readily provide at all times

$$J(\tau) = 1 - S(\tau) - V(\tau) = R(\tau) + D(\tau) + I(\tau). \quad (14)$$

Moreover, Equation (11a) yields

$$I(\tau) = -b(\tau) - \frac{d \ln S(\tau)}{d\tau} = -\frac{dV(\tau)/d\tau}{1 - J(\tau) - V(\tau)} + \frac{d}{d\tau} \ln(1 - J(\tau) - V(\tau)) = \frac{j(\tau)}{1 - J(\tau) - V(\tau)}, \quad (15)$$

where we used Equations (11e), (14) and the first Equation (12). Equation (14) also provides

$$R(\tau) + D(\tau) = J(\tau) - I(\tau) = J(\tau) - \frac{j(\tau)}{1 - J(\tau) - V(\tau)}. \quad (16)$$

With Equation (15) we obtain for Equations (11c)–(11d)

$$R(\tau) = \int_0^\tau dx k(x)I(x) = \int_0^\tau dx \frac{k(x)j(x)}{1 - J(x) - V(x)}, \quad (17)$$

and

$$D(\tau) = \int_0^\tau dx q(x)I(x) = \int_0^\tau dx \frac{q(x)j(x)}{1 - J(x) - V(x)}, \quad (18)$$

implying for the rate of new fatalities

$$d(\tau) = \frac{dD(\tau)}{d\tau} = q(\tau)I(\tau) = \frac{q(\tau)j(\tau)}{1 - J(\tau) - V(\tau)}. \quad (19)$$

2.4. Solution of the SIRVD Equations

With the first Equation (14) one finds

$$S(\tau) = 1 - J(\tau) - V(\tau), \quad (20)$$

so that Equation (11e) can be written in the form

$$b(\tau) = \frac{dV/d\tau}{1 - J(\tau) - V(\tau)}, \quad (21)$$

yielding

$$b(\tau)[1 - J(\tau)] = \frac{dV(\tau)}{d\tau} + b(\tau)V(\tau) = e^{-\int_0^\tau dx b(x)} \frac{d}{d\tau} [V(\tau)e^{\int_0^\tau dx b(x)}]. \quad (22)$$

With the initial condition $V(\tau = 0) = 0$ Equation (22) integrates to

$$V(\tau) = 1 - J(\tau) + e^{-\int_0^\tau dx b(x)} \left[\int_0^\tau dx j(x) e^{\int_0^x dy b(y)} - (1 - \eta) \right], \quad (23)$$

providing

$$S(\tau) = 1 - J(\tau) - V(\tau) = e^{-\int_0^\tau dx b(x)} \left[1 - \eta - \int_0^\tau dx j(x) e^{\int_0^x dy b(y)} \right]. \quad (24)$$

Likewise Equation (11b) can be written as

$$k(\tau) + q(\tau) = S(\tau) - \frac{d \ln I(\tau)}{d\tau} = 1 - V(\tau) - J(\tau) - \frac{d}{d\tau} \ln \left[\frac{j(\tau)}{1 - V(\tau) - J(\tau)} \right], \quad (25)$$

where we used Equations (15) and (24). With the initial conditions Equation (25) integrates to

$$j(\tau) = \frac{dJ(\tau)}{d\tau} = \eta [1 - V(\tau) - J(\tau)] \exp \int_0^\tau dz \left(1 - V(z) - J(z) - k(z) - q(z) \right). \quad (26)$$

A further integration with the initial condition $J(\tau = 0) = \eta$ leads to

$$J(\tau) = \eta \left[1 + \int_0^\tau dx S(x) e^{\int_0^x dz [S(z) - k(z) - q(z)]} \right] \quad (27)$$

in terms of $S(\tau)$. Furthermore, Equation (25) is equivalent to

$$k(\tau) + q(\tau) = S(\tau) - \frac{d}{d\tau} [\ln j(\tau) - \ln S(\tau)], \quad (28)$$

and also with Equation (11b) integrated to

$$b(\tau) = -\frac{d \ln S(\tau)}{d\tau} - \eta \exp \left(\int_0^\tau dz [S(z) - k(z) - q(z)] \right). \quad (29)$$

With $S(\tau) = (1 - \eta) \exp(-\int_0^\tau dz [I(z) + b(z)])$ obtained from Equation (11a), the first Equation (25) is equivalent to

$$\frac{d \ln I(\tau)}{d\tau} = (1 - \eta) e^{-\int_0^\tau dz [I(z) + b(z)]} - k(\tau) - q(\tau). \quad (30)$$

The derived Equations (26)–(30) are nonlinear integro-differential equations for the cumulative fraction of new infections $J(\tau)$, and $S(\tau)$, respectively. The great advantage of the SIRVD equation written in the form (26) is the direct involvement of observable and monitored quantities, such the cumulative fractions of new infections $J(t) = J(\tau)$, and of vaccinated persons $V(t) = V(\tau)$. We emphasize that Equations (26)–(29) are exact, and hold for all, the SIR, SIRV, SIRD, and SIRVD models. The only difference is that in the SIRD case $J_{\text{SIRD}}(\tau) = 1 - S_{\text{SIRD}}(\tau)$, because here $b(\tau) = V(\tau) = 0$, whereas in the SIRVD case $J_{\text{SIRVD}}(\tau) = 1 - S_{\text{SIRVD}}(\tau) - V_{\text{SIRVD}}(\tau)$. If we succeed in either solving the nonlinear integro-differential Equations (26)–(29), or deriving an accurate approximation for their solution, we arrive at a completely analytical solution of all dynamical variables of the SIRVD model and its special cases in dependence on the reduced time τ .

For completeness we note that inserting the exact solution (23) for $V(\tau)$ in Equation (26) leads to the equivalent nonlinear integro-differential Equations for the rate of new infections

$$j(\tau) = \eta \left[1 - \eta - \int_0^\tau dx j(x) e^{\int_0^x dy b(y)} \right] \times \exp \int_0^\tau dz \left([1 - \eta - \int_0^z dx j(x) e^{\int_0^x dy b(y)}] e^{-\int_0^z dy b(y)} - k(z) - q(z) - b(z) \right). \quad (31)$$

Before proceeding to the approximation we note that in terms of the real time, the Eqs. (21)–(26) read, with the help of Equations (9), (10), (12), (14), (15), (17), (18), and (31),

$$v(t) = \frac{dV/dt}{1 - J(t) - V(t)}, \quad (32a)$$

$$V(t) = 1 - J(t) + e^{-\int_0^t dx v(x)} \left[\int_0^t dx \dot{J}(x) e^{\int_0^x dy v(y)} - (1 - \eta) \right], \quad (32b)$$

$$I(t) = \frac{\dot{J}(t)}{a(t)[1 - J(t) - V(t)]} = \frac{\dot{J}(t) e^{\int_0^t dx v(x)}}{a(t)[1 - \eta - \int_0^t dx \dot{J}(x) e^{\int_0^x dy v(y)}]}, \quad (32c)$$

$$R(t) = \int_0^t dt' \frac{\mu(t') \dot{J}(t')}{a(t')[1 - J(t') - V(t')]} = \int_0^t dt' \frac{\mu(t') \dot{J}(t') e^{\int_0^{t'} dx v(x)}}{a(t')[1 - \eta - \int_0^{t'} dx \dot{J}(x) e^{\int_0^x dy v(y)}]}, \quad (32d)$$

$$D(t) = \int_0^t dt' \frac{\psi(t') \dot{J}(t')}{a(t')[1 - J(t') - V(t')]} = \int_0^t dt' \frac{\psi(t') \dot{J}(t') e^{\int_0^{t'} dx v(x)}}{a(t')[1 - \eta - \int_0^{t'} dx \dot{J}(x) e^{\int_0^x dy v(y)}]}, \quad (32e)$$

$$d(t) = \frac{\psi(t) \dot{J}(t)}{a(t)[1 - J(t) - V(t)]} = \frac{\psi(t) \dot{J}(t) e^{\int_0^t dx v(x)}}{a(t)[1 - \eta - \int_0^t dx \dot{J}(x) e^{\int_0^x dy v(y)}]}, \quad (32f)$$

$$\begin{aligned} \dot{J}(t) &= a(t)[1 - J(t) - V(t)] \exp \int_0^t dx \left(a(x)[1 - V(x) - J(x)] - \mu(x) - \psi(x) \right) \\ &= a(t)[1 - \eta - \int_0^t dx \dot{J}(x) e^{\int_0^x dy v(y)}] \exp \int_0^t dt' \left(a(t') e^{-\int_0^{t'} dy v(y)} [1 - \eta \right. \\ &\quad \left. - \int_0^{t'} dx \dot{J}(x) e^{\int_0^x dy v(y)}] - \mu(t') - \psi(t') - v(t') \right). \end{aligned} \quad (32g)$$

In some aspects for negligible vaccinations the resulting SIRD-model is simpler than the SIRVD-model, e.g. here the simpler relation $J(\tau) = 1 - S(\tau)$ holds. As a consequence the general integro-differential equations (26)–(30) derived before are eased. In Appendix B we explicitly list the corresponding equations for the SIRD model.

In the following sections we will derive a class of special exact solutions (Sections 3–4) and derive approximate analytical solutions of Equations (21) and (25) in the limit of small $J(\tau) \ll 1$ (Sect. 5) following our earlier approach [21]. This approximation then leads to analytical approximations of all fractions of the SIRVD epidemics model as a function of time for given time dependencies of the three ratios (10). We will prove its accuracy of this approach by comparing with the exact numerical solutions

of these equations for two illustrative examples (Sect. 6.1–6.2) of the reduced time dependence of these ratios. The proposed analytical approximation is self-regulating as the final analytical expression for the cumulative fraction $J_\infty = \lim_{t \rightarrow \infty} J(t)$ after infinite time allows us to check the validity of the original assumption $J(t) = J(\tau) \leq J_\infty \ll 1$.

Before proceeding we discuss the differences in calculating the fractions of recovered and deceased persons in the different models.

2.5. Fraction of Deceased Persons

The main difference between the considered compartment models occurs for the determination of the fraction of deceased persons $D(\tau) = D(t)$ and the corresponding death rate $d(\tau) = dD(\tau)/d\tau$ and $d(t) = (dD(t)/dt)/a(t)$ as a function of the reduced and real time. The disparity is most pronounced if the real time dependence of the fatality rate $\psi(t)$ and the recovery rate $\mu(t)$ are different from each other. In the SIRVD and SIRD cases with a prescribed fatality rate $\psi(t)$, corresponding to the ratio $q(\tau)$, the death rate is proportional to $I(t)$ as given correctly by Equations (18)–(19) and Equations (32e)–(32f). Moreover, the different reduced time dependences of the ratios $k(\tau)$ and $q(\tau)$ correctly enter the dynamical Equations (26)–(29).

However, in the SIR models no compartment of deceased persons is considered. As mentioned before, see Equations (4)–(5), here the total fraction of recovered and removed (by death) populations $R_{\text{tot}}(t)$ and the summed recovery/removed rate $\mu_{\text{tot}}(t)$ are introduced. With the solution for $\dot{J}_{\text{SIR}}(t)$ and $J_{\text{SIR}}(t)$ the rate of new fatalities and the fraction of deceased persons are then calculated a posteriori as [6]

$$d_{\text{SIR}}(t) = \alpha \dot{J}_{\text{SIR}}(t), \quad D_{\text{SIR}}(t) = \alpha J_{\text{SIR}}(t), \quad (33)$$

with $\alpha = D_\infty/J_\infty$. The difference to Equations (32e)–(32f), which involve $I(t) = \dot{J}(t)/[1 - J(t)]$ and not directly $\dot{J}(t)$, is obvious. Only if the temporal dependence of $I(t)$ is not drastically different from the temporal dependence of $\dot{J}(t)$, the a-posteriori approach is justified. As has been emphasized before [21], for COVID-19 outbursts in many countries the monitored cumulative fraction of infected persons $J(t) \ll 1$ has been much smaller than unity at all times, so that then in the SIR model indeed $I(t) \simeq j(t)$.

While Equation (33) refers to past work, we will in the following allow for time-dependent fatality rates $\psi(t)$ so that the a-posteriori death rate is given by $d_{\text{a-pos}}(t) = \psi(t)\dot{J}(t)$ corresponding to

$$d_{\text{a-pos}}(\tau) = q(\tau)j(\tau) \quad (34)$$

as a function of reduced time. This way, as opposed to the setting (33), the cumulative $D_{\text{a-pos}}$ at infinite time must not coincide with D_∞ . Moreover, in the a-posteriori approach the influence of the later introduced fatality rate $\psi(t)$ on the dynamical SIR equations is ignored. This is particularly pronounced if the real time dependence of $\psi(t)$ differs from the real time dependence of the recovery rate $\mu(t)$. We will elaborate on this below with an illustrative example in Section 6.2.

3. Special Exact Solutions

Equations (28)–(31) are complicated integro-differential equations in the SIRVD and SIRD case, respectively, for given reduced time variations of the ratios $k(\tau)$, $q(\tau)$ and $b(\tau)$. However, they can also be regarded as simpler determining Equations for the ratios $k(\tau) + q(\tau) = \kappa(\tau)$ for given variations of the ratio $b(\tau)$ and the fraction $S(\tau)$. This can be used to derive fully exact analytical solutions for the SIRVD and SIRD models.

We know that $S(\tau)$ starts from the initial values $S(\tau = 0) = 1 - \eta$ and monotonically decreases to its final nonnegative value $S(\tau = \infty) \geq 0$ after finite or infinite time. We also require, in accord with Equation (12) and the initial conditions specified in Section 2.3, that

$$j(\tau = 0) = \eta(1 - \eta). \quad (35)$$

Therefore we adopt the reduced time variation

$$S(\tau) = \frac{1 - \eta + S_\infty \tanh \frac{\tau_{\max}}{\tau_0} - (1 - \eta - S_\infty) \tanh \frac{\tau - \tau_{\max}}{\tau_0}}{1 + \tanh \frac{\tau_{\max}}{\tau_0}}. \quad (36)$$

parameterized by S_∞ , τ_{\max} , and τ_0 . While $\lim_{\tau \rightarrow \infty} S(\tau) = S_\infty$ is formally correct, $S(\tau)$ may reach zero after finite time τ_{fin} . In that case $\lim_{\tau \rightarrow \infty} S(\tau) = S(\tau_{\text{fin}}) = 0$, irrespective of the value of the parameter S_∞ , that may therefore take positive or negative values in the expression (36). One has¹

$$\tau_{\text{fin}} = \tau_{\max} + \tau_0 \tanh^{-1} \left[\frac{1 - \eta + S_\infty \tanh(\tau_{\max}/\tau_0)}{1 - \eta - S_\infty} \right] \quad (37)$$

from Equation (36). Only if the argument of the \tanh^{-1} resides in the interval $[-1, 1]$, a finite τ_{fin} exists. We are going to see that the special choice of $S_\infty = 0$ has to be treated with care; it will allow us to absorb with Equation (36), along with a particular choice for τ_0 , the analytic solution of the SI model, for which $S(\tau)$ reaches S_∞ at $\tau_{\text{fin}} = \infty$. Moreover, the initial condition $j(0) = \eta(1 - \eta)$ will be used to establish a relationship between S_∞ , τ_{\max} , and τ_0 .

We adopt without loss of generality positive values of $\tau_0 > 0$. The choice (36) implies

$$\frac{dS(\tau)}{d\tau} = -\frac{1 - \eta - S_\infty}{\tau_0 [1 + \tanh \frac{\tau_{\max}}{\tau_0}] \cosh^2 \frac{\tau - \tau_{\max}}{\tau_0}}, \quad (38a)$$

$$\frac{d \ln S(\tau)}{d\tau} = -\frac{1 - \eta - S_\infty}{\tau_0 \cosh^2 \frac{\tau - \tau_{\max}}{\tau_0} (1 - \eta + S_\infty \tanh \frac{\tau_{\max}}{\tau_0} - [1 - \eta - S_\infty] \tanh \frac{\tau - \tau_{\max}}{\tau_0})}, \quad (38b)$$

$$\frac{d \ln \frac{dS(\tau)}{d\tau}}{d\tau} = -\frac{2 \tanh(\frac{\tau - \tau_{\max}}{\tau_0})}{\tau_0}. \quad (38c)$$

With the first Equation (15) we obtain for the dynamical SIRVD equation (28)

$$k(\tau) + q(\tau) = \kappa(\tau) = S(\tau) - \frac{d}{d\tau} \ln \left(-b(\tau) + \frac{d \ln S(\tau)}{d\tau} \right). \quad (39)$$

After inserting Equations (36) and (38b) this Equation becomes

$$\begin{aligned} \kappa(\tau) = & \frac{1 - \eta + S_\infty \tanh \frac{\tau_{\max}}{\tau_0} - (1 - \eta - S_\infty) \tanh \frac{\tau - \tau_{\max}}{\tau_0}}{1 + \tanh \frac{\tau_{\max}}{\tau_0}} - \frac{d}{d\tau} \ln \left(-b(\tau) \right. \\ & \left. + \frac{1 - \eta - S_\infty}{\tau_0 \cosh^2 \frac{\tau - \tau_{\max}}{\tau_0} (1 - \eta + S_\infty \tanh \frac{\tau_{\max}}{\tau_0} - [1 - \eta - S_\infty] \tanh \frac{\tau - \tau_{\max}}{\tau_0})} \right). \end{aligned} \quad (40)$$

For given reduced time variations $b(\tau)$ the combined rate (40) corresponding to the fraction $S(\tau)$ in Equation (36) can be inferred. In the following we simplify our analysis to the SIRD model.

3.1. SIRD Model

The choice (36) implies for the SIRD model $J(\tau) = 1 - S(\tau)$, $J_\infty = 1 - S_\infty$ and

$$j(\tau) = -\frac{dS(\tau)}{d\tau} = \frac{1 - \eta - S_\infty}{\tau_0 [1 + \tanh \frac{\tau_{\max}}{\tau_0}] \cosh^2 \frac{\tau - \tau_{\max}}{\tau_0}}, \quad (41a)$$

$$j(\tau = 0) = \frac{(1 - \eta - S_\infty)(1 - \tanh \frac{\tau_{\max}}{\tau_0})}{\tau_0}. \quad (41b)$$

¹ Throughout this work we use the notation $\tanh^{-1}(x) = \operatorname{artanh}(x)$.

The rate (41a) is of generalized SI-type (see Equation (A5)) with a width τ_0 different from 2 and a general τ_{\max} different from $\ln(1-\eta)/\eta$. We thus investigate for which conditions generalized SI-type rates exactly solve the SIRDequations.

The requirement (35) demands

$$S_\infty = (1-\eta)\left[1 - \frac{\eta\tau_0}{1 - \tanh\frac{\tau_{\max}}{\tau_0}}\right], \quad (42)$$

$$J_\infty = \eta + \frac{\eta(1-\eta)\tau_0}{1 - \tanh\frac{\tau_{\max}}{\tau_0}} = \eta + \frac{j(\tau=0)\tau_0}{1 - \tanh\frac{\tau_{\max}}{\tau_0}}. \quad (43)$$

We emphasize that the ansatz (41a) includes the SI model as special case. Inserting the SI-values $S_\infty = 0$, $\kappa(0) = 0$, $\tau_0 = 2$ and $\tau_{\max} = 2 \tanh^{-1}(1-2\eta)$, which follows from Equation (42) for $S_\infty = 0$, it is straightforward to show that Equation (41a) correctly reproduces the SI-distribution (A5).

The first Equation (41a) then can be written as

$$j(\tau) = \frac{\eta(1-\eta) \cosh^2\frac{\tau_{\max}}{\tau_0}}{\cosh^2\frac{\tau-\tau_{\max}}{\tau_0}} = j(\tau=0) \frac{\cosh^2\frac{\tau_{\max}}{\tau_0}}{\cosh^2\frac{\tau-\tau_{\max}}{\tau_0}}. \quad (44)$$

Only for $\tau_{\max} \gg \tau_0$ the maximum rate of new infections at $\tau = \tau_{\max}$ is much larger than the initial value $j(\tau=0)$. In this limit

$$J_\infty \simeq \frac{\eta(1-\eta)\tau_0 e^{\frac{2\tau_{\max}}{\tau_0}}}{2}, \quad (45)$$

while Equation (39) for $b(\tau) = 0$ simplifies to

$$\kappa(\tau) = S(\tau) - \frac{d}{d\tau} \ln\left(-\frac{d \ln S(\tau)}{d\tau}\right). \quad (46)$$

Within the remainder of this subsection, we use the simplifying abbreviations

$$T = \frac{\tau}{\tau_0}, \quad \rho = \frac{\tau_{\max}}{\tau_0}, \quad Y(\tau) = T - \rho \quad (47)$$

to derive expressions for $\kappa(0)$ and $\kappa(\infty)$ for the two qualitatively different cases of $S_\infty = 0$ and $S_\infty \neq 0$. With the help of Equation (47) the SIRDequation (36) receives the form

$$S(\tau) = \frac{1-\eta + S_\infty \tanh \rho - (1-\eta - S_\infty) \tanh Y}{1 + \tanh \rho}, \quad (48)$$

or equivalently, upon replacing S_∞ using Equation (42),

$$\begin{aligned} S(\tau) &= (1-\eta) \left[1 - \eta\tau_0 \cosh^2 \rho (\tanh(T-\rho) + \tanh \rho) \right] \\ &= (1-\eta) \left[1 - \frac{\eta\tau_0}{\coth T - \tanh \rho} \right]. \end{aligned} \quad (49)$$

Similarly, using Equation (38c) in Equation (46), $\kappa(\tau)$ becomes

$$\begin{aligned} \kappa(\tau) &= \frac{2 \tanh(Y)}{\tau_0} + \frac{1-\eta + S_\infty \tanh \rho - (1-\eta - S_\infty) \tanh(Y)}{1 + \tanh \rho} \\ &\quad - \frac{1-\eta - S_\infty}{\tau_0 \cosh^2(Y) (1-\eta + S_\infty \tanh \rho - [1-\eta - S_\infty] \tanh(Y))}. \end{aligned} \quad (50)$$

Using $Y(0) = -\rho$, the initial value $\kappa(0)$ can be read off from Equation (50). This yields

$$\begin{aligned}\kappa(0) &= 1 - \eta + \frac{S_\infty(1 - \tanh \rho) - (1 - \eta)(1 + \tanh \rho)}{(1 - \eta)\tau_0}, \\ &= 1 - 2\eta - \frac{2 \tanh \rho}{\tau_0} = 1 - 2\eta - \frac{2 \tanh\left(\frac{\tau_{\max}}{\tau_0}\right)}{\tau_0},\end{aligned}\quad (51)$$

where we inserted S_∞ from (42) to arrive at the 2nd line in Equation (51). Expression (51) is valid for any S_∞ .

As long as $S_\infty \neq 0$, the final value $\kappa_\infty = \lim_{Y \rightarrow \infty} \kappa(\tau)$ can be also read off immediately from Equation (50). While the last term in Equation (50) diminishes with increasing Y due to the leading $\cosh^2(Y)$, the first terms readily evaluate upon replacing $\tanh(Y)$ by unity, so that

$$\begin{aligned}\kappa_\infty &= \frac{2}{\tau_0} + S_\infty \quad (S_\infty \neq 0) \\ &= \frac{2}{\tau_0} + (1 - \eta) \left[1 - \frac{\eta\tau_0}{1 - \tanh\left(\frac{\tau_{\max}}{\tau_0}\right)} \right],\end{aligned}\quad (52)$$

where we made use again of S_∞ from (42). Calculating κ_∞ for the remaining case of $S_\infty = 0$ requires more care, as the denominator in the last line of Equation (50) does not anymore increase with increasing Y . For $S_\infty = 0$, one instead finds

$$\begin{aligned}\kappa_\infty &= \frac{2}{\tau_0} - \frac{1}{\tau_0} \lim_{Y \rightarrow \infty} \frac{1}{\cosh^2(Y)(1 - \tanh(Y))} \\ &= \frac{2}{\tau_0} - \frac{1}{\tau_0} \lim_{Y \rightarrow \infty} (1 + \tanh Y) = \frac{2}{\tau_0} - \frac{2}{\tau_0} = 0\end{aligned}\quad (53)$$

Note the apparent qualitative difference between the two cases. While $\kappa_\infty = S_\infty$ for $S_\infty = 0$, one has $\kappa_\infty = S_\infty + 2/\tau_0$ for $S_\infty \neq 0$.

3.2. Constraints on the Function $\kappa(\tau)$

We recall that values of the function $\kappa(\tau)$ smaller than unity describe the epidemic phase where the infection rate $a(t)$ is larger than the sum of the recovery and death rate. Hence if still enough susceptible persons are available one expects a rising rate of new infections $\dot{J}(t)$. In the opposite case of values of the function $\kappa(\tau)$ greater than unity the sum of recovery and death rates outnumbers the infection rate so that the rate of new infections will decrease in such a phase. Therefore it is appropriate to start with values of the function $\kappa(\tau)$ smaller than unity at small reduced times. Subsequently, the function $\kappa(\tau)$ approaches the value κ_∞ at infinitely large reduced times which can be either smaller or greater than unity depending on the chosen values of τ_{\max} and τ_0 . However, not all values for τ_0 and τ_{\max} are allowed.

The requirement of having a positive $\kappa(0) \geq 0$ leads to

$$\frac{1 - 2\eta}{2} \tau_0 \geq \tanh \frac{\tau_{\max}}{\tau_0}\quad (54)$$

This is automatically fulfilled for values of

$$\tau_0 > \frac{2}{1 - 2\eta},\quad (55)$$

as the right-hand-side of Equation (55) is always smaller or equal than unity. For values of $\tau_0 \leq 2/(1-2\eta)$ it is required that

$$\tau_{\max} < \tau_0 \tanh^{-1} \left[\frac{1-2\eta}{2} \tau_0 \right]. \quad (56)$$

The inequality $S_\infty \geq 0$, corresponding to $J_\infty \leq 1$, is met as long as the following inequalities hold,

$$\tanh \frac{\tau_{\max}}{\tau_0} \leq 1 - \eta \tau_0, \quad (57)$$

$$\tau_{\max} \leq \tau_0 \tanh^{-1}(1 - \eta \tau_0) \simeq \frac{\tau_0}{2} \ln \frac{2}{\eta \tau_0} = \sqrt{\ln \frac{2}{\eta \tau_0}} \tau_0, \quad (58)$$

that follow from Equation (42). This condition (58), the regime between red and blue dashed lines in Figure 3, is not compatible with condition (56) but holds for certain values of $\tau_0 > 2/(1-2\eta)$. The condition (57) further guarantees that also $S(\tau)$, and not only S_∞ , is non-negative at all times because $S \geq 0$ requires, according to Equation (49),

$$\tanh \rho + \tanh(T - \rho) \leq \frac{1}{\eta \tau_0 \cosh^2 \rho} = \frac{1 - \tanh^2 \rho}{\eta \tau_0}, \quad (59)$$

or

$$\frac{\tanh \rho + \tanh(T - \rho)}{1 + \tanh \rho} \leq \frac{1 - \tanh \rho}{\eta \tau_0}, \quad (60)$$

which is fulfilled for *all* times τ because the left-hand side is always smaller than unity while the right-hand side is larger than unity due to condition (57). In cases $S_\infty < 0$, where the condition (57) is not fulfilled, $S(\tau_{\text{fin}}) = 0$ vanishes at the finite time τ_{fin} already stated in Equation (37). In this case the chosen solution (36) or (49) can only be used in the finite time interval $0 \leq \tau \leq \tau_{\text{fin}}$.

Equation (50) can also be written as

$$\begin{aligned} \kappa(\tau) &= \frac{2}{\tau_0} \tanh(T - \rho) + (1 - \eta) [1 - \eta \tau_0 \cosh^2 \rho (\tanh(T_\rho) + \tanh \rho)] \\ &\quad - \frac{\eta \cosh^2 \rho}{\cosh^2(T - \rho) [1 - \eta \tau_0 \cosh^2 \rho (\tanh(T_\rho) + \tanh \rho)]} \\ &= \frac{2}{\tau_0} \tanh(T - \rho) + (1 - \eta) \left[1 - \frac{\eta \tau_0}{\coth T - \tanh \rho} \right] - \frac{\eta \cosh^2 \rho}{\cosh^2(T - \rho) \left[1 - \frac{\eta \tau_0}{\coth T - \tanh \rho} \right]}, \end{aligned} \quad (61)$$

where we used the identity

$$\cosh^2 \rho [\tanh(T_\rho) + \tanh \rho] = \frac{1}{\coth T - \tanh \rho}. \quad (62)$$

The function (61) is positive for $S_\infty \geq 0$ and non-negative for all times in the admissible interval $0 \leq \tau \leq \tau_{\text{fin}}$. The ratio $\kappa(\tau)$ is negative and contains singularities if it is used in the regime $\tau > \tau_{\text{fin}}$.

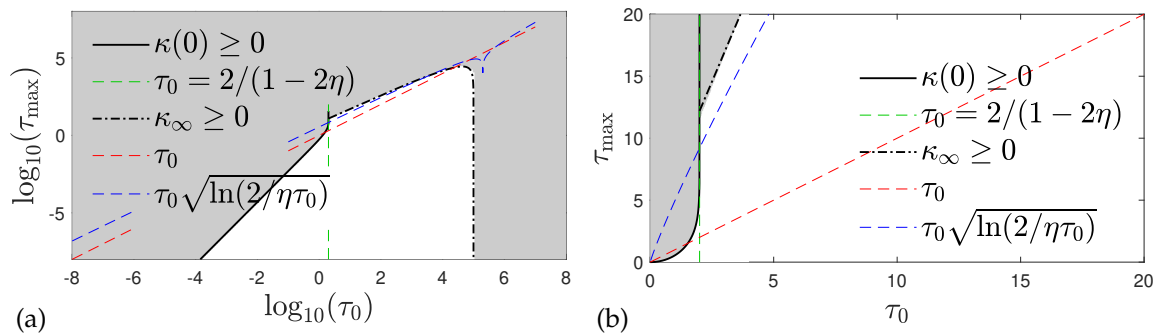


Figure 3. SIRD model. Region (white) of admissible (τ_0, τ_{\max}) pairs in the expression (36) for $S(\tau)$ at $\eta = 10^{-5}$. The situation is qualitatively identical at different η . The white region is enclosed by the solutions to $\kappa(0) = 0$ and $\kappa_{\infty} = 0$. Negative τ_0 and τ_{\max} are prohibited to ensure $S_{\infty} < 1$ and $\kappa_0 \geq 0$. The dashed vertical line corresponds to Equation (55), the solid line represents Equation (56), and the dot-dashed line follows from Equation (52). (a) Wide range of (τ_0, τ_{\max}) using a double-logarithmic scale, (b) Zoom into the region close to $\tau_0 = 2/(1 - 2\eta)$. The inequality (57), relevant for the case where $j(\tau)$ achieves a pronounced maximum at $\tau > 0$, is met between blue and red dashed lines.

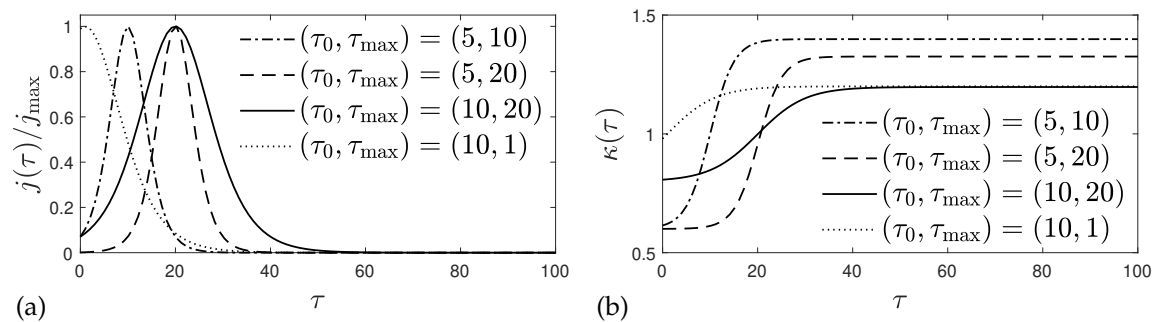


Figure 4. SIRD model. (a) Analytical solutions $j(\tau)$ (44) of the SIRD model for four different $\kappa(\tau)$ shown in (b), at $\eta = 10^{-5}$. All four selected (τ_0, τ_{\max}) pairs reside within the admissible white region highlighted in Figure 3. In (a), $j(\tau)$ is normalized by $j_{\max} = \eta(1 - \eta) \cosh^2(\tau_{\max}/\tau_0)$. In all four cases, $J_{\infty} \ll 1$, to be more specific: $J_{\infty} = 0.0014$ (dot-dashed), 0.075 (dashed), 0.0028 (solid), and 0.00012 (dotted).

4. Details of the Construction of the SIRD Solution

From Equation (51) we obtain, for every S_{∞} ,

$$\tanh\left(\frac{\tau_{\max}}{\tau_0}\right) = \frac{1 - 2\eta - \kappa(0)}{2} \tau_0, \quad (63)$$

with positive $\tau_0 > 0$. We note that this Equation has a solution provided

$$1 - 2\eta - \frac{2}{\tau_0} \leq \kappa(0) \leq 1 - 2\eta + \frac{2}{\tau_0}, \quad (64)$$

because then the right-hand side of Equation (63) lies within the interval $[-1, 1]$. While $\kappa_{\infty} = 0$ for $S_{\infty} = 0$, inserting Equation (63) provides for Equation (52),

$$\kappa_{\infty} = \frac{2}{\tau_0} + \frac{(1 - \eta)[\frac{2}{\tau_0} + \kappa(0) - 1]}{\frac{2}{\tau_0} + \kappa(0) - 1 + 2\eta} \quad (S_{\infty} \neq 0). \quad (65)$$

Setting $y = 2/\tau_0$, Equation (65) leads to the quadratic equation

$$y^2 + (\kappa(0) - \kappa_{\infty} + \eta)y = \kappa_{\infty}(\kappa(0) - 1 + 2\eta) - (1 - \eta)(\kappa(0) - 1). \quad (66)$$

For general and different values of $\kappa(0)$ und κ_∞ one can use Equation (66) to determine the implied value of $\tau_0 = 2/y$ and with Equation (63) the resulting value of τ_{\max} . The knowledge of τ_0 and τ_{\max} then determines for the SIRD model the time variation of the ratio $\kappa(\tau)$ for any value of S_∞ and also of the rate of new infections $j(\tau)$ in Equation (44). We thus have found an effective new method to construct a special class of exact solutions for the SIRD model which also applies to the SIR model for $\psi(t) = 0$. We illustrate this new method for several cases of the ratios $\kappa(0)$ and κ_∞ in the next subsections.

4.1. SIRD Solution for $\kappa_\infty = 0$

As discussed there are two cases for which $\kappa_\infty = 0$ is realized. If $S_\infty = 0$, then $\tau_{\inf} = \infty$ due to Equation (37), and

$$\tanh(\rho) = 1 - \eta\tau_0 = \frac{1 - 2\eta - \kappa(0)}{2}\tau_0, \quad (67)$$

according to Equations (42) and (63). This Equation (67) determines τ_0 in terms of $\kappa(0)$, i.e.,

$$\tau_0 = \frac{2}{1 - \kappa(0)}. \quad (S_\infty = \kappa_\infty = 0) \quad (68)$$

With τ_0 at hand, τ_{\max} is then also determined by Equation (67). To be specific,

$$\tau_{\max} = \frac{2 \tanh^{-1}[1 - 2\eta/(1 - \kappa(0))]}{1 - \kappa(0)}. \quad (69)$$

For the special choice of $\kappa(0) = \kappa_\infty = S_\infty = 0$, one therefore recovers with $\tau_0 = 2$ and $\tau_{\max} = \ln((1 - \eta)/\eta)$ the above-mentioned solution of the SI model detailed in Appendix A.

If, on the other hand, $S_\infty = -2/\tau_0$ is negative, Equation (63), valid for all S_∞ , yields

$$\tau_{\max} = \tau_0 \tanh^{-1} \frac{1 - 2\eta - \kappa(0)}{2}\tau_0, \quad (70)$$

so that τ_{\inf} from Equation (37) is finite and given by

$$\begin{aligned} \tau_{\text{fin}} &= \tau_{\max} + \tau_0 \tanh^{-1} \left(\frac{(\eta + \kappa(0))\tau_0}{2 + (1 - \eta)\tau_0} \right) \\ &= \tau_0 \tanh^{-1} \left(\frac{1 - 2\eta - \kappa(0)}{2}\tau_0 \right) + \tau_0 \tanh^{-1} \left(\frac{(\eta + \kappa(0))\tau_0}{2 + (1 - \eta)\tau_0} \right). \end{aligned} \quad (71)$$

τ_0 is also determined by $\kappa(0)$, as it solves Equation (66) for $\kappa_\infty = 0$, which then simplifies to

$$y^2 + (\kappa(0) + \eta)y = (1 - \eta)(1 - \kappa(0)). \quad (72)$$

The quadratic equation (72) can be solved for $y = 2/\tau_0$ and thus provides

$$\tau_0 = \frac{4}{\sqrt{\kappa^2(0) - 2(2 - 3\eta)\kappa(0) + (2 - \eta)^2 - [\kappa(0) + \eta]}'}, \quad (73)$$

because the 2nd solution leads to negative τ_0 . The τ_{\max} is then also determined by $\kappa(0)$, c.f., Equation (71). For the special choice of $\kappa(0) = \kappa_\infty = 0$, the above simplifies to

$$\tau_0 = \frac{2}{1-\eta}, \quad S_\infty = -(1-\eta), \quad (74a)$$

$$\tau_{\max} = \frac{2}{1-\eta} \tanh^{-1} \left[1 - \frac{\eta}{1-\eta} \right] = \frac{\ln \frac{2-3\eta}{\eta}}{1-\eta} \simeq \frac{\ln(2/\eta)}{1-\eta}, \quad (74b)$$

$$\begin{aligned} \tau_{\text{fin}} &= \frac{2}{1-\eta} \left[\tanh^{-1} \frac{1-2\eta}{1-\eta} + \tanh^{-1} \frac{\eta}{2(1-\eta)} \right] \\ &= \frac{1}{1-\eta} \left[\ln \frac{2-3\eta}{\eta} + \ln \frac{2-\eta}{\eta} \right] \simeq \frac{2[\ln \frac{2}{\eta} - \eta]}{1-\eta}. \end{aligned} \quad (74c)$$

The results of the present section for the extremal case of $\kappa(0) = 0$ are visualized in Figure 5.

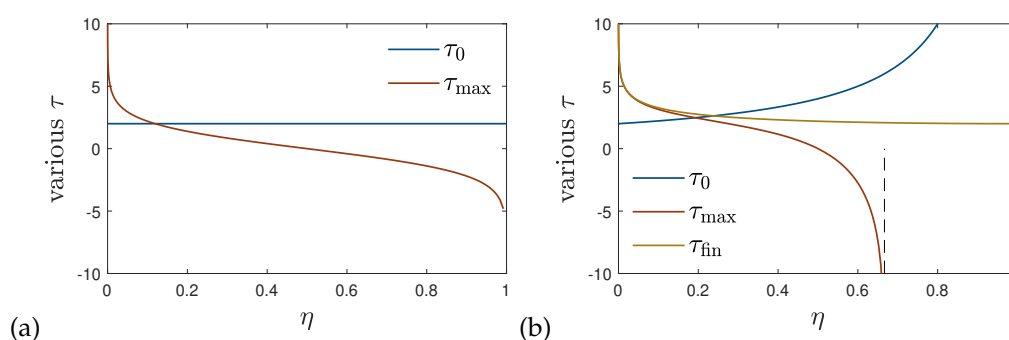


Figure 5. The case of $\kappa_\infty = \kappa(0) = 0$ and (a) $S_\infty = 0$ (SI model, here $\tau_{\text{inf}} = \infty$) and (b) negative $S_\infty = -2/\tau_0$, according to Equation (74c). In the limit $\eta \rightarrow 0$, the two solutions approach each other, while they do not coincide in the limit $S_\infty \rightarrow 0$. For $\eta > 2/3$, τ_{\max} is complex-valued because the argument of the logarithm is negative in Equation (74c) for larger η ; the solution for negative S_∞ therefore requires $\eta \in (0, 2/3]$, while the solution for $S_\infty = 0$ is valid for any $\eta \in (0, 1]$.

We have thus presented the analytic solutions of the SIRD model for the case of $\kappa_\infty = 0$ and arbitrary $\kappa(0)$. There is one solution for which S approaches zero at infinite time, and there is another solution for which S reaches zero at finite time τ_{fin} (71). In both cases the characteristic times τ_0 and τ_{\max} , as well as S_∞ appearing in the analytic expression (36) for $S(\tau)$ are determined by the initial dimensionless rate $\kappa(0)$ and $\eta = 1 - S(0)$.

4.2. SIRD Solution for Equal $\kappa(0) = \kappa_\infty \equiv K \neq 0$

For equal values of $\kappa(0) = \kappa_\infty \equiv K \neq 0$ Equation (66) reduces to

$$y^2 + \eta y = K^2 - (2 - 3\eta)K + (1 - \eta), \quad (75)$$

with the two solutions

$$y_{1,2} = -\frac{\eta}{2} \pm \sqrt{f(K)}, \quad f(K) = K^2 - (2 - 3\eta)K + \left(1 - \frac{\eta}{2}\right)^2. \quad (76)$$

The functions $f(K) > 0$ is positive for all values of $K > 0$ and has the slope

$$\frac{df(K)}{dK} = 2\left[K - \left(1 - \frac{3}{2}\eta\right)\right]. \quad (77)$$

It therefore decreases for $0 < K \leq K_0$ with $K_0 = 1 - (3\eta/2)$, where it attains its minimum $f_{\min} = 2\eta(1 - \eta)$. For values $K \geq K_0$ the function $f(K)$ is monotonically increasing. For all values of K one obtains $\sqrt{f(K)} \geq \sqrt{f_{\min}} > (\eta/2)$ because $\eta \ll (8/9)$. Hence only the solution

$$y_1(K) = \sqrt{f(K)} - \frac{\eta}{2} = \sqrt{K^2 - (2 - 3\eta)K + (1 - \frac{\eta}{2})^2} - \frac{\eta}{2} \quad (78)$$

is useful as it provides positive values of

$$\tau_0(K) = \frac{2}{y_1(K)} = \frac{2}{\sqrt{K^2 - (2 - 3\eta)K + (1 - \frac{\eta}{2})^2} - \frac{\eta}{2}}. \quad (79)$$

We first check the requirement (64) reading

$$-y_1(K) \leq K - 1 + 2\eta \leq y_1(K), \quad (80)$$

or

$$-[\sqrt{f(K)} - \frac{\eta}{2}] \leq K - 1 + 2\eta \leq \sqrt{f(K)} - \frac{\eta}{2}. \quad (81)$$

The left-hand-side of the inequality (81) can be written as

$$-\sqrt{(K - K_0)^2 + 2\eta(1 - \eta)} \leq K - K_0, \quad (82)$$

and is fulfilled for all values of $K \geq 0$. This is obvious for $K \geq K_0$ when the right-hand side of Equation (82) is nonnegative, whereas its left-hand side is negative. For values $0 \leq K < K_0$ Equation (82) reads

$$K_0 - K \leq \sqrt{(K_0 - K)^2 + 2\eta(1 - \eta)}, \quad (83)$$

which is fulfilled. Likewise, the right-hand-side of the inequality (81) can be written as

$$K - (K_0 - \eta) \leq \sqrt{(K - K_0)^2 + 2\eta(1 - \eta)}, \quad (84)$$

which is fulfilled for values of $K \in (0, K_0 - \eta]$, when the left-hand side of Equation (84) is negative while its right-hand side is positive. Recall that the case $K = 0$ had been treated in section 4.1. For large values $K > K_0 - \eta$ squaring the inequality (84) yields

$$2(K - K_0) \leq 2 - 3\eta = 2K_0, \quad (85)$$

or

$$K \leq 2K_0. \quad (86)$$

We conclude that the constraint (81) can be fulfilled for all values of $K \in (0, 2K_0]$. In this interval the solution (79) is given by

$$\tau_0(0 < K \leq 2K_0) = \frac{2}{\sqrt{K^2 - (2 - 3\eta)K + (1 - \frac{\eta}{2})^2} - \frac{\eta}{2}} = \frac{2}{\sqrt{(K - K_0)^2 + 2\eta(1 - \eta)} - \frac{\eta}{2}}, \quad (87)$$

and shown in Figure 6. The first derivative of Equation (87) is

$$\frac{d\tau_0(K)}{dK} = -\frac{df/dK}{\sqrt{f(k)}(\sqrt{f(K)} - \frac{\eta}{2})^2} = \frac{2(K_0 - K)}{\sqrt{f(k)}(\sqrt{f(K)} - \frac{\eta}{2})^2}, \quad (88)$$

so that $\tau_0(K)$ attains its maximum value

$$\tau_{0,E} = \frac{\sqrt{\frac{2}{\eta}}}{\sqrt{1-\eta} - \sqrt{\frac{\eta}{8}}} = \frac{4}{\sqrt{8\eta(1-\eta)} - \eta} = \frac{4}{8-9\eta} \left[1 + \sqrt{\frac{8(1-\eta)}{\eta}} \right] \simeq \sqrt{\frac{2}{\eta}}, \quad (89)$$

at $K = K_0$. Inserting the solution (87) one obtains for Equation (63)

$$\tanh \frac{\tau_{\max}}{\tau_0(K)} = \frac{1-2\eta-K}{2} \tau_0(K) = \frac{1-2\eta-K}{\sqrt{(K-K_0)^2 + 2\eta(1-\eta)} - \frac{\eta}{2}}, \quad (90)$$

yielding

$$\tau_{\max}(0 < K \leq 2K_0) = \frac{2 \tanh^{-1} \left[\frac{1-2\eta-K}{\sqrt{(K-K_0)^2 + 2\eta(1-\eta)} - \frac{\eta}{2}} \right]}{\sqrt{(K-K_0)^2 + 2\eta(1-\eta)} - \frac{\eta}{2}}. \quad (91)$$

The solution (91), also shown in Figure 6, is positive for values of $0 < K \leq 1 - 2\eta$ and negative for values of $1 - 2\eta < K \leq 2K_0$ due to the property $\tanh^{-1}(-x) = -\tanh^{-1}(x)$. Obviously $\tau_{\max} = 0$ for $K = 1 - 2\eta$. In order to have positive values of K_0 and the zero $1 - 2\eta$ we should consider only values of $\eta < 0.5$.

For completeness we note an alternative $\tau_{\max}(\tau_0)$. Equating the right hand sides of Equations (51) and (52) leads with $\mathcal{R} \equiv \tanh(\rho) = \tanh(\tau_{\max}/\tau_0)$ to

$$1 - 2\eta - \frac{2\mathcal{R}}{\tau_0} = \frac{2}{\tau_0} + (1-\eta) \left[1 - \frac{\eta\tau_0}{1-\mathcal{R}} \right]. \quad (92)$$

Upon multiplying with $(1-\mathcal{R})\tau_0$ one obtains

$$(1-\mathcal{R})[(1-2\eta)\tau_0 - 2\mathcal{R}] = 2(1-\mathcal{R}) + (1-\eta)(1-\eta\tau_0 - \mathcal{R})\tau_0, \quad (93)$$

or the quadratic equation

$$\mathcal{R}^2 + \frac{\eta\tau_0}{2} \mathcal{R} = 1 + \frac{\eta\tau_0}{2} [1 - (1-\eta)\tau_0], \quad (94)$$

which is solved by

$$\mathcal{R} = \frac{\pm \sqrt{16 + \eta\tau_0[8 - (8-9\eta)\tau_0]} - \eta\tau_0}{4}, \quad (95)$$

so that

$$\tau_{\max} = \tau_0 \tanh^{-1} \left[\frac{\pm \sqrt{16 + \eta\tau_0[8 - (8-9\eta)\tau_0]} - \eta\tau_0}{4} \right]. \quad (96)$$

The requirement $|\mathcal{R}| \leq 1$ is fulfilled for all values of $\eta < 1$ if the argument of the square root in Equation (95) is nonnegative. The last condition leads to

$$\tau_0 \leq \frac{4}{8-9\eta} \left[1 + \sqrt{\frac{8(1-\eta)}{\eta}} \right] = \tau_{0,E}, \quad (97)$$

which is identical to the maximum value (89) derived before. Proof:

$$\begin{aligned} \tau_{0,E} &= \frac{\sqrt{\frac{2}{\eta}}}{\sqrt{1-\eta} - \sqrt{\frac{\eta}{8}}} = \frac{4}{\sqrt{\eta}[\sqrt{8(1-\eta)} - \sqrt{\eta}]} = \frac{4[\sqrt{8(1-\eta)} + \sqrt{\eta}]}{\sqrt{\eta}[8(1-\eta) - \eta]} \\ &= \frac{4}{8-9\eta} \frac{\sqrt{\eta} + \sqrt{8(1-\eta)}}{\sqrt{\eta}} = \frac{4}{8-9\eta} \left(1 + \sqrt{\frac{8(1-\eta)}{\eta}} \right) = \tau_{0,E}. \end{aligned} \quad (98)$$

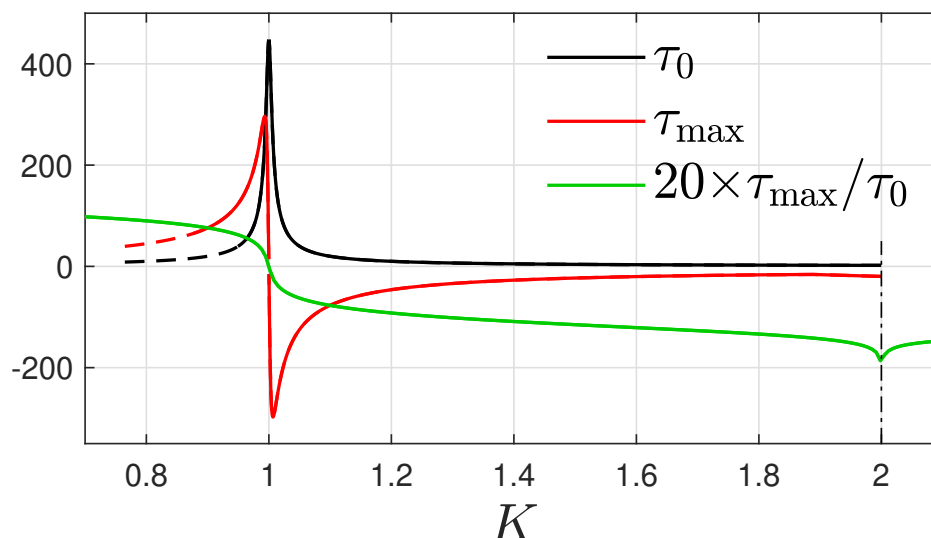


Figure 6. SIRD model at basically constant $\kappa(\tau) = K$. The analytical solution of the SIRD model at $K = \kappa(0) = \kappa_\infty$ for $K \in [0, 2K_0]$ with $K_0 = 1 - 3\eta/2$ is given by Equation (36) with S_∞ , τ_{\max} , and τ_0 according to Equations (43), (96), and (47). This figure shows τ_0 (79), τ_{\max} (91), as well as $\rho = \tau_{\max}/\tau_0$ (90) versus K . The dot-dashed vertical line marks $K = 2K_0 = 2 - 3\eta$. For $K < 1 - 2\eta$, the plus sign applies in Equation (96), leading to positive τ_0 and τ_{\max} . In that case $j(\tau)$ goes through a maximum in the course of positive time $\tau > 0$. For $K > K_0$, the minus sign applies in Equation (96). Here, $\tau_{\max} < 0$ and $j(\tau)$ monotonically decreases at $\tau \geq 0$. At $K = K_0$, τ_0 goes through a maximum versus K , the maximum value $\tau_{0,E} \approx \sqrt{2/\eta}$ is given by Equation (89). Within the range of K values marked by a solid line, $\kappa(\tau)$ equals K at all times $\tau \geq 0$ with a precision of less than 0.1%, while within the region marked by dashed lines the $\kappa(\tau)$ deviates from K by less than 5%. The analytical solution therefore captures the regime $K \in [0.8, 2K_0]$ at $\eta = 10^{-5}$ and the regime extends to slightly smaller K for smaller η .

4.3. Reduced time dependence of $\kappa(\tau)$, terminal time $\tau_{\text{fin}}(K)$ for $K = \kappa(0) = \kappa_\infty \neq 0$.

With $\tau_0(K)$ given by Equation (87) we obtain for Equations (47)

$$T = \frac{\tau}{\tau_0(K)}, \quad \rho(K) = \frac{\tau_{\max}}{\tau_0(K)} = \tanh^{-1} \frac{1 - 2\eta - K}{\sqrt{(K - K_0)^2 + 2\eta(1 - \eta) - \frac{\eta}{2}}}, \quad (99)$$

so that Equations (49) and (61) become

$$S(\tau) = (1 - \eta) \left[1 - \frac{\eta \tau_0(K)}{\coth T - \tanh \rho(K)} \right], \quad (100)$$

and

$$\kappa(\tau) \simeq \frac{2}{\tau_0(K)} \tanh [T - \rho(K)] + (1 - \eta) \left[1 - \frac{\eta \tau_0(K)}{\coth T(K) - \tanh \rho(K)} \right] - \frac{\eta \cosh^2 \rho(K)}{\cosh^2(T - \rho(K)) \left[1 - \frac{\eta \tau_0(K)}{\coth T(K) - \tanh \rho(K)} \right]}, \quad (101)$$

which are both shown in Figure 7 for different values of K entering $\rho(K)$ and $\tau_0(K)$. As $K \neq 0$ the requirement $S(\tau_{\text{fin}}) = 0$ then provides from Equation (100)

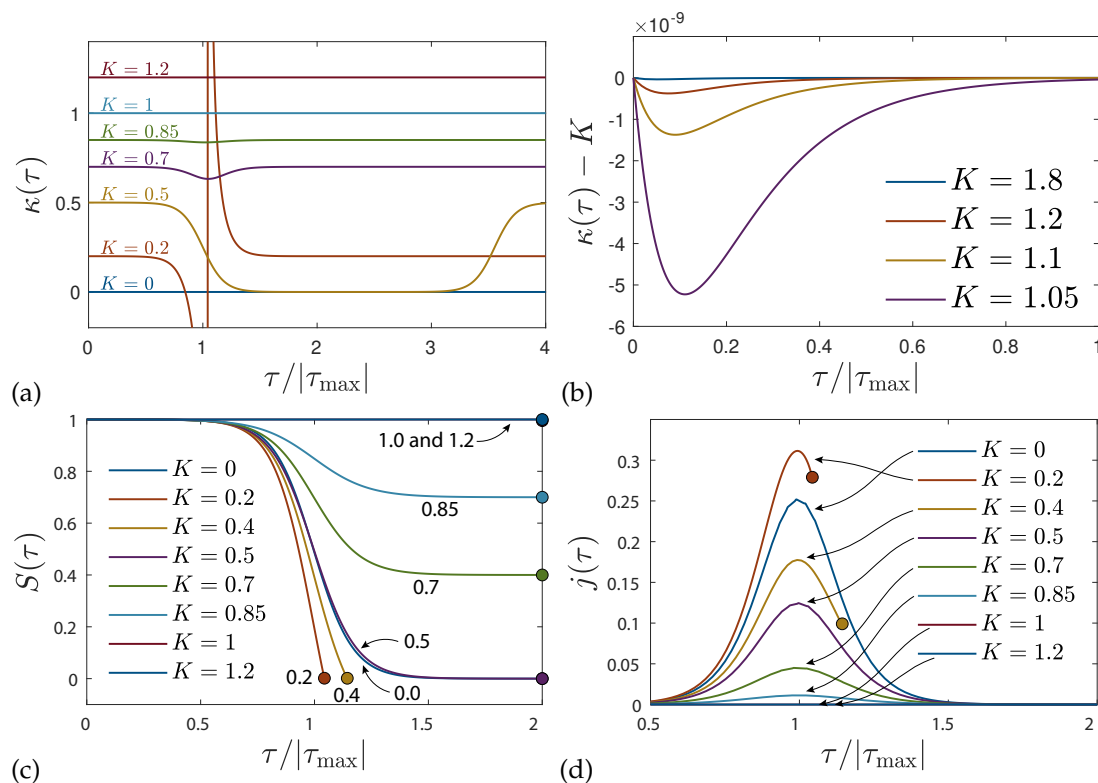


Figure 7. SIRD model. (a) $\kappa(\tau)$ for $S(\tau)$ of the form of Equation (36), subject to the condition $\kappa(0) = \kappa_\infty \equiv K$ at $\eta = 10^{-5}$. While for $K < K_0$ the $\kappa(\tau)$ varies significantly with reduced time τ , for $K > K_0$ the form (36) solves the SIRD equations with constant $\kappa(\tau)$ nearly exactly. Lines in (a) are given by Equation (109c), which coincides with the numerical solution. Panel (b) offers a zoom into (a) for $K_0 < K < 2K_0$. Shown is the numerical solution for $\kappa(\tau) - K$, which departs from the constant by completely negligible amounts. (c) $S(\tau)$ and (d) $j(\tau)$. For $K < 1/2$, $S(\tau)$ reaches zero at τ_{fin} , the curves for $K = 0$ (SI model) and $K = 1/2$ nearly coincide as they have similar τ_{max} and share $S_\infty = 0$, the curves for $K = 1$ and $K = 1.2$ are also indistinguishable by eye and stay at nearly constant $S \approx 1 - \eta$. The bullets mark $S(\tau_{\text{fin}})$ (not S_∞) in (c), and $j(\tau_{\text{fin}})$ in (d).

$$\begin{aligned} \tau_{\text{fin}}(K) &= \tau_0(K) \coth^{-1}[\eta\tau_0(K) + \tanh \rho(K)] = \tau_0(K) \coth^{-1} \left[\frac{1-K}{2} \tau_0(K) \right] \\ &= \frac{2}{\sqrt{(K-K_0)^2 + 2\eta(1-\eta)} - \frac{\eta}{2}} \tanh^{-1} \frac{\sqrt{(K-K_0)^2 + 2\eta(1-\eta)} - \frac{\eta}{2}}{1-K}, \end{aligned} \quad (102)$$

where we used Equation (67) for $\kappa(0) = K$ and inserted solution (57) for $0 < K \leq 2K_0$. Obviously, positive values of $\tau_{\text{fin}}(K)$ are only possible for values of $K < 1$ smaller than unity, as otherwise the argument of the \tanh^{-1} -function is negative. In order for the argument of the \tanh^{-1} -function to be less or equal unity the condition

$$\sqrt{(K-K_0)^2 + 2\eta(1-\eta)} \leq \left(1 + \frac{\eta}{2}\right) - K \quad (103)$$

is required, which is equivalent to

$$K \leq \frac{1}{2}. \quad (104)$$

Hence, finite values of $\tau_{\text{fin}}(K)$ only occur for values of $K \in (0, 0.5]$. In Figure 8 we show the final time (102) for different values of K below 0.5. The final time is monotonically decreasing from its infinitely large value above $K = 0.5$ with decreasing values of K .

Particular interesting in Figure 7 are the cases where the combined ratio $\kappa(\tau)$ at the start and the end of the epidemic outburst have values below $K \leq 0.5$ which corresponds to infection rates being twice as large as the sum of the recovery and fatality rate. In this case the epidemic outburst, described by the SI-type $\cosh^{-2}[(\tau - \tau_{\text{max}})/\tau_0]$ -distribution for the rate of new infections shown in panel 7-d, is so dominated by the rapid infections that at the finite reduced time τ_{fin} the outburst suddenly terminates as with $S(\tau_{\text{fin}}) = 0$ (as seen in panel 7-c) no more persons are available to be infected. The situation is comparable to a smooth running car where suddenly the car engine stops as no more fuel is available. For values greater than $K > 0.5$ the epidemic outburst lasts infinitely long.

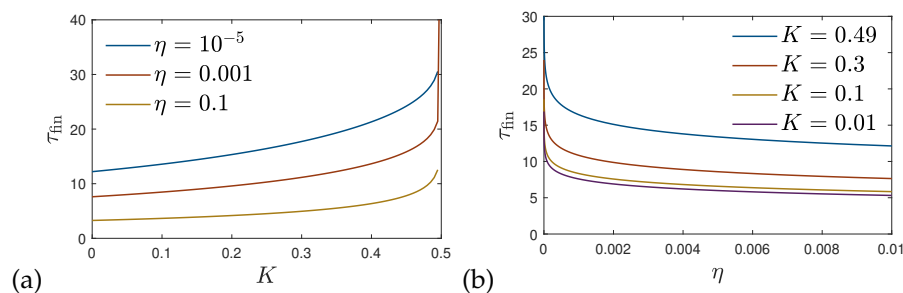


Figure 8. Final time τ_{fin} (102) for the case of $K = \kappa(0) = \kappa_{\infty} \neq 0$ (Section 4.3) for (a) different values of η versus K , and (b) different values of $K < 1/2$ versus η .

Next, we consider the limits of Equations (101) and (102) for small values of $\eta \ll 1$.

4.4. Limit for Very Small Values of $I(0) = \eta \ll 1$

We use

$$\tanh \rho(K) = \frac{K_0 - K - \frac{\eta}{2}}{\sqrt{(K - K_0)^2 + 2\eta(1 - \eta) - \frac{\eta}{2}}}, \quad (105a)$$

$$\tau_0(K) = \frac{2}{\sqrt{(K - K_0)^2 + 2\eta(1 - \eta) - \frac{\eta}{2}}}, \quad (105b)$$

and Equation (102). For small values of $\eta \ll 1$ we have to distinguish between the cases (i) where $|K - K_0| \leq \sqrt{2\eta}$ and (ii) where $|K - K_0| > \sqrt{2\eta}$. We consider both cases in turn.

4.4.1. Case $|K - K_0| \leq \sqrt{2\eta}$

Here we approximate for small values of $\eta \ll 1$

$$\begin{aligned} \sqrt{(K - K_0)^2 + 2\eta(1 - \eta) - \frac{\eta}{2}} &\simeq \sqrt{2\eta(1 - \eta)} \left[1 + \frac{(K - K_0)^2}{2\eta(1 - \eta)} \right] - \frac{\eta}{2} \\ &\simeq \sqrt{2\eta} \left[1 + \frac{(K - K_0)^2}{2\eta} - \sqrt{\frac{\eta}{8}} \right]. \end{aligned} \quad (106)$$

Consequently, we obtain

$$\tanh \rho(K) \simeq \frac{[1 - 2\eta - K][1 - \frac{(K-K_0)^2}{2\eta}]}{\sqrt{2\eta}}, \quad (107a)$$

$$\tau_0(K) \simeq \sqrt{\frac{2}{\eta}} \left[1 - \frac{(K-K_0)^2}{2\eta} \right], \quad (107b)$$

$$\begin{aligned} \tau_{\max}(K) &\simeq \sqrt{\frac{2}{\eta}} \left[1 - \frac{(K-K_0)^2}{2\eta} \right] \tanh^{-1} \frac{1 - 2\eta - K}{\sqrt{2\eta}} \\ &= \frac{1 - \frac{(K-K_0)^2}{2\eta}}{\sqrt{2\eta}} \ln \frac{\sqrt{2\eta} + (1 - 2\eta - K)}{\sqrt{2\eta} - (1 - 2\eta - K)}, \end{aligned} \quad (107c)$$

whereas $\tau_{\text{fin}} = 0$ as all K -values in this interval are greater than 0.5.

4.4.2. Case $|K - K_0| > \sqrt{2\eta}$

Here we approximate

$$\sqrt{(K - K_0)^2 + 2\eta(1 - \eta)} - \frac{\eta}{2} \simeq |K_0 - K| - \frac{\eta}{2} + \frac{\eta(1 - \eta)}{|K_0 - K|}, \quad (108)$$

to obtain for Equations (105) and (102)

$$\tanh \rho(K) \simeq \frac{K_0 - K - \frac{\eta}{2}}{|K - K_0| - \frac{\eta}{2} + \frac{\eta(1 - \eta)}{|K_0 - K|}}, \quad (109a)$$

$$\tau_0(K) \simeq \frac{2}{|K_0 - K| - \frac{\eta}{2} + \frac{\eta(1 - \eta)}{|K_0 - K|}}, \quad (109b)$$

$$\tau_{\text{fin}}(K) \simeq \frac{2}{|K_0 - K| - \frac{\eta}{2} + \frac{\eta(1 - \eta)}{|K_0 - K|}} \tanh^{-1} \left[\frac{|K - K_0| - \frac{\eta}{2} + \frac{\eta(1 - \eta)}{|K_0 - K|}}{1 - K} \right]. \quad (109c)$$

4.4.3. Finite Time $\tau_{\text{fin}}(K)$

As shown before, c.f. Equation (104), finite values of the finite time only occur for values of $K \leq 0.5 < K_0$. Consequently for small $\eta \ll 1$ we approximate with $K_0 = 1 - (3/2)\eta$

$$\begin{aligned} \tau_{\text{fin}}(K) &\simeq \frac{2}{K_0 - K - \frac{\eta}{2} + \frac{\eta(1 - \eta)}{K_0 - K}} \tanh^{-1} \left[\frac{K_0 - K - \frac{\eta}{2} + \frac{\eta(1 - \eta)}{K_0 - K}}{1 - K} \right] \\ &= \frac{2}{1 - K - 2\eta + \frac{\eta(1 - \eta)}{K_0 - K}} \tanh^{-1} \left[\frac{1 - K - 2\eta + \frac{\eta(1 - \eta)}{K_0 - K}}{1 - K} \right] \\ &\simeq \frac{2}{1 - K - \frac{\eta[2(K_0 - K) - 1]}{K_0 - K}} \tanh^{-1} \left[1 - \frac{\eta[2(K_0 - K) - 1]}{(K_0 - K)(1 - K)} \right] \\ &= \frac{1}{1 - K - \frac{\eta[2(K_0 - K) - 1]}{K_0 - K}} \ln \left[\frac{2(K_0 - K)(1 - K) - \eta[2(K_0 - K) - 1]}{\eta[2(K_0 - K) - 1]} \right] \\ &\simeq \frac{1}{1 - K} \ln \frac{2(K_0 - K)(1 - K)}{\eta[2(K_0 - K) - 1]}. \end{aligned} \quad (110)$$

Equation (110) only provides real values if the denominator of the ln-function is positive, leading to the requirement

$$K < K_0 - \frac{1}{2} = \frac{1 - 3\eta}{2}, \quad (111)$$

which is consistent with the earlier limit (104) and the time (111) can be further approximated as

$$\tau_{\text{fin}}(K) \simeq \frac{1}{1 - K} \ln \frac{2(1 - K)^2}{\eta(1 - 2K)}. \quad (112)$$

The function (112) monotonically decreases from its infinite large values above $(1 - \eta)/2$ with decreasing values of K in agreement with Figure 8.

4.4.4. Values $K < K_0 - \sqrt{2\eta}$

For values of $K < K_0 - \sqrt{2\eta}$ one obtains

$$\tanh \rho(K) = \frac{1}{1 + \frac{\eta(1-\eta)}{(K_0-K)(K_0-K-\frac{\eta}{2})}} \simeq 1 - \frac{\eta(1-\eta)}{(K_0-K)^2}, \quad (113a)$$

$$\tau_0(K) \simeq \frac{2}{K_0 - K} \left[1 - \frac{\eta(2 + K - K_0)}{2(K_0 - K)^2} \right], \quad (113b)$$

$$\tau_{\text{max}}(K) \simeq \frac{1}{K_0 - K} \ln \frac{2(K_0 - K)^2}{\eta}. \quad (113c)$$

With

$$\cosh^2 \rho = \frac{1}{1 - \tanh^2 \rho} = \frac{1}{1 - \left[1 - \frac{\eta(1-\eta)}{(K_0-K)^2} \right]^2} \simeq \frac{(K_0 - K)^2}{2\eta(1 - \eta)} \quad (114)$$

Equation (101) becomes

$$\begin{aligned} \kappa(\tau) \simeq & 1 - \eta + (K_0 - K) \tanh(T - \rho) - \frac{2\eta(1 - \eta)}{K_0 - K} (\coth T - \tanh \rho) \\ & - \frac{(K_0 - K)^2}{2(1 - \eta) \cosh^2(T - \rho) \left[1 - \frac{2\eta(1-\eta)}{K_0-K} (\coth T - \tanh \rho) \right]}, \end{aligned} \quad (115)$$

which correctly approaches

$$\kappa(\tau = 0) = 1 - \eta - (K_0 - K) \tanh \rho - \frac{(K_0 - K)^2}{2(1 - \eta) \cosh^2 \rho} \simeq 1 - (K_0 - K) = K. \quad (116)$$

For values of $(1 - 3\eta)/2 < K < K_0 - \sqrt{2\eta}$ we find

$$\begin{aligned} \kappa(\tau = \infty) &= 1 - \eta + (K - K_0) \tanh \rho - \frac{2\eta(1 - \eta)}{(K_0 - K)[1 - \tanh \rho]} \\ &\simeq 1 + K - K_0 - 2(K_0 - K) = 1 - K_0 + K = K, \end{aligned} \quad (117)$$

because for small $\eta \ll 1$ one has $K_0 \simeq 1$. The solution (117) holds for all times τ in the range $(1 - 3\eta)/2 \leq K \leq K_0 = 1 - (3/2)\eta - \sqrt{2\eta}$. For smaller values of $K < (1 - 3\eta)/2$ the solution (117) holds only at finite times $\tau < \tau_{\text{fin}}(K)$ given in Equation (112).

4.4.5. Values $K_0 + \sqrt{2\eta} < K \leq 2K_0$

For values of $K_0 + \sqrt{2\eta} < K \leq 2K_0$ we obtain

$$\tau_0(K) \simeq \frac{2}{K - K_0}, \quad (118a)$$

$$\tanh \rho(K) \simeq -\frac{1}{1 + \frac{\eta}{K - K_0 + \frac{\eta}{2}} \frac{1 + K_0 - K - \eta}{K - K_0}} \simeq -\left[1 - \frac{\eta(1 + K_0 - K)}{(K - K_0)^2}\right], \quad (118b)$$

$$\tau_{\max}(K) \simeq -\frac{1}{K - K_0} \ln \frac{2(K - K_0)^2}{\eta(1 + K_0 - K)} \quad (118c)$$

where the last step in Equation (118b) holds for values of $K < 2 - (5\eta/2)$, which is justified for all values of $K > K_0$ as the maximum value $2K_0 = 2 - 3\eta$ is smaller than $2 - (5\eta/2)$. Consequently, one obtains in this case for

$$\cosh^2 \rho = \frac{1}{1 - \tanh^2 \rho} \simeq \frac{(K_0 - K)^2}{2\eta(1 + K_0 - K - \eta)}, \quad (119)$$

so that

$$\eta(1 - \eta)\tau_0 \cosh^2 \rho \simeq \frac{(1 - \eta)(K - K_0)}{1 + K_0 - K}. \quad (120)$$

We also note that for $K > 1 - 2\eta$ the function $\rho(K) = -r(K)$ is negative with

$$r(K) = \tanh^{-1} \frac{1}{1 + \frac{\eta}{K - K_0 + \frac{\eta}{2}} \frac{1 + K_0 - K - \eta}{K - K_0}} \simeq \tanh^{-1} \left[1 - \frac{\eta(1 + K_0 - K)}{(K - K_0)^2}\right], \quad (121)$$

so that Equation (101) becomes

$$\begin{aligned} \kappa(\tau) &\simeq \frac{2}{\tau_0} \tanh(T + r) + (1 - \eta) \left[1 - \eta\tau_0 \cosh^2 r (\tanh(T + r) - \tanh r)\right] \\ &\quad - \frac{\eta \cosh^2 r}{\cosh^2(T + r) [1 - \eta\tau_0 \cosh^2 r (\tanh(T + r) - \tanh r)]} \\ &\simeq (K - K_0) \tanh(T + r) + (1 - \eta) \left[1 - \frac{K - K_0}{1 + K_0 - K} (\tanh(T + r) - \tanh r)\right] \\ &\quad - \frac{(K - K_0)^2}{2 \cosh^2(T + r) [1 + K_0 - K - (K - K_0)(\tanh(T - r) - \tanh r)]} \end{aligned} \quad (122)$$

One notices from Figure 6 that $r(K) \gg 1$ is very large compared to unity, so that Equation (122) with $\tanh(T + r) \simeq \tanh r \simeq 1$ and $\cosh^{-2}(T + r) \simeq 0$ simplifies to the constant

$$\kappa(\tau) \simeq K - K_0 + 1 = K. \quad (123)$$

4.5. SIRD Solution for $\kappa(0) = 0$

For $\kappa(0) = 0$ Equation (66) for $y = 2/\tau_0$ reduces to

$$y^2 - (\kappa_\infty - \eta)y = 1 - \eta - (1 - 2\eta)\kappa_\infty, \quad (124)$$

with the two solutions

$$y_1 = \frac{1}{2} [\kappa_\infty - \eta + \sqrt{(\kappa_\infty - 2 + 3\eta)^2 + 8\eta(1 - \eta)}], \quad (125a)$$

$$y_2 = \frac{1}{2} [\kappa_\infty - \eta - \sqrt{(\kappa_\infty - 2 + 3\eta)^2 + 8\eta(1 - \eta)}]. \quad (125b)$$

We restrict our analysis to the interesting range of values of $0 < \kappa_\infty < 2 - 3\eta$ ($\kappa_\infty = 0$ was treated in Section 4.1 already) and investigate the limit of small $\eta \ll 1$. We then approximate

$$\sqrt{(2 - 3\eta - \kappa_\infty)^2 + 8\eta(1 - \eta)} \simeq 2 - 3\eta - \kappa_\infty + \frac{4\eta(1 - \eta)}{2 - \kappa_\infty - 3\eta}, \quad (126)$$

implying

$$y_1 \simeq 1 - 2\eta \frac{1 - \kappa_\infty}{2 - \kappa_\infty}, \quad (127a)$$

$$y_2 = \kappa_\infty - 1 - \frac{\eta\kappa_\infty}{2 - \kappa_\infty}, \quad (127b)$$

Accordingly,

$$\tau_{0,1} \simeq \frac{2}{1 - 2\eta \frac{1 - \kappa_\infty}{2 - \kappa_\infty}} \simeq 2 \left[1 + 2\eta \frac{1 - \kappa_\infty}{2 - \kappa_\infty} \right], \quad (128a)$$

$$\tau_{0,2} \simeq \frac{2}{\kappa_\infty - 1} \left[1 + \frac{\eta\kappa_\infty}{(2 - \kappa_\infty)(\kappa_\infty - 1)} \right]. \quad (128b)$$

As τ_0 has to be positive the solution (128b) can only be used for values of $1 < \kappa_\infty < 2 - 3\eta$.

For $\kappa(0) = 0$ Equation (63) reads $\tau_{\max} = \tau_0 \tanh^{-1}[(1 - 2\eta)\tau_0/2]$.

The two solutions (128) then provide

$$\begin{aligned} \tau_{\max,1} &\simeq 2 \left[1 + 2\eta \frac{1 - \kappa_\infty}{2 - \kappa_\infty} \right] \tanh^{-1} \left[1 - \frac{2\eta}{2 - \kappa_\infty} \right] \\ &\simeq \left[1 + 2\eta \frac{1 - \kappa_\infty}{2 - \kappa_\infty} \right] \ln \frac{2 - \kappa_\infty - \eta}{\eta} \simeq \ln \frac{2 - \kappa_\infty}{\eta}, \end{aligned} \quad (129a)$$

$$\begin{aligned} \tau_{\max,2} &= \frac{2}{\kappa_\infty - 1} \left[1 + \frac{\eta\kappa_\infty}{(2 - \kappa_\infty)(\kappa_\infty - 1)} \right] \tanh^{-1} \left[\frac{1 - 2\eta}{\kappa_\infty - 1} \left(1 + \frac{\eta\kappa_\infty}{(2 - \kappa_\infty)(\kappa_\infty - 1)} \right) \right] \\ &\simeq \frac{2}{\kappa_\infty - 1} \tanh^{-1} \frac{1}{\kappa_\infty - 1}. \end{aligned} \quad (129b)$$

The argument of the \tanh^{-1} has to be in the interval $(-1, 1)$. The requirement $(\kappa_\infty - 1)^{-1} > -1$ is fulfilled for every positive $\kappa_\infty > 1$. However, the requirement $(\kappa_\infty - 1)^{-1} < 1$ is only possible for values of $\kappa_\infty > 2$ in contradiction to the earlier assumption $\kappa_\infty \leq 2 - 3\eta$. Therefore the second solution $\tau_{\max,2}$ and $\tau_{0,2}$ cannot be used. The only possible solution is this range of $0 < \kappa_\infty \leq 2 - 3\eta$ is

$$\tau_0(\kappa_\infty) = \tau_{0,1}(\kappa_\infty) \simeq 2 \left[1 + 2\eta \frac{1 - \kappa_\infty}{2 - \kappa_\infty} \right], \quad (130a)$$

$$\tau_{\max}(\kappa_\infty) = \tau_{\max,1} = \tau_0(\kappa_\infty) \tanh^{-1} \left[\frac{1 - 2\eta}{2} \tau_0(\kappa_\infty) \right] \simeq 2 \left[1 + 2\eta \frac{1 - \kappa_\infty}{2 - \kappa_\infty} \right], \quad (130b)$$

$$\rho(\kappa_\infty) = \tanh^{-1} \left[\frac{1 - 2\eta}{2} \tau_0(\kappa_\infty) \right] = \tanh^{-1} \left[(1 - 2\eta) \left(1 + 2\eta \frac{1 - \kappa_\infty}{2 - \kappa_\infty} \right) \right]. \quad (130c)$$

Consequently we obtain

$$\tanh \rho(\kappa_\infty) = 1 - \frac{2\eta}{2 - \kappa_\infty} - 4\eta^2 \frac{1 - \kappa_\infty}{2 - \kappa_\infty} \simeq 1 - \frac{2\eta}{2 - \kappa_\infty}, \quad (131)$$

$$1 - \tanh \rho(\kappa_\infty) \simeq \frac{2\eta}{2 - \kappa_\infty}, \quad (132)$$

$$\cosh^2 \rho(\kappa_\infty) \simeq \frac{1}{1 - \left[1 - \frac{2\eta}{2 - \kappa_\infty} \right]^2} \simeq \frac{2 - \kappa_\infty}{4\eta}. \quad (133)$$

One then obtains for Equation (65) in this case

$$\begin{aligned} \kappa(\tau) \simeq & \frac{2 \tanh(T - \rho(\kappa_\infty))}{\tau_0(\kappa_\infty)} \\ & + (1 - \eta)[1 - \eta \tau_0(\kappa_\infty) \cosh^2 \rho(\kappa_\infty) [\tanh(T - \rho(\kappa_\infty)) + \tanh \rho(\kappa_\infty)]] \\ & - \frac{\eta \cosh^2 \rho(\kappa_\infty)}{\cosh^2(T - \rho(\kappa_\infty)) [1 - \eta \tau_0(\kappa_\infty) (\tanh(T - \rho(\kappa_\infty)) + \tanh \rho(\kappa_\infty))]} \end{aligned} \quad (134)$$

Here, and in the following two equations, T and ρ stand for $\tau/\tau_0(\kappa_\infty)$ and $\rho(\kappa_\infty) = \tau_{\max}(\kappa_\infty)/\tau_0(\kappa_\infty)$ with $\tau_0(\kappa_\infty)$, $\tau_{\max}(\kappa_\infty)$, and $\rho(\kappa_\infty)$ given by Equations (130). The temporal evolution of $\kappa(\tau)$ is shown in Figure 8 for various values of $\kappa_\infty \in [0, 2]$. Equation (134) correctly reproduces

$$\kappa(\tau = 0) = 1 - 2\eta - \frac{2 \tanh \rho}{\tau_0} = 1 - 2\eta - 2 \frac{1 - 2\eta}{2} = 0, \quad (135)$$

$$\begin{aligned} \kappa(\tau = \infty) &= \frac{2}{\tau_0(\kappa_\infty)} + (1 - \eta) \left[1 - \frac{\eta \tau_0}{1 - \tanh \rho(\kappa_\infty)} \right] \\ &\simeq \frac{2}{\tau_0(\kappa_\infty)} + (1 - \eta) \left[1 - \frac{2 - \kappa_\infty}{2} \tau_0(\kappa_\infty) \right] \simeq \kappa_\infty \end{aligned} \quad (136)$$

with $\tau_0(\kappa_\infty) \simeq 2$.

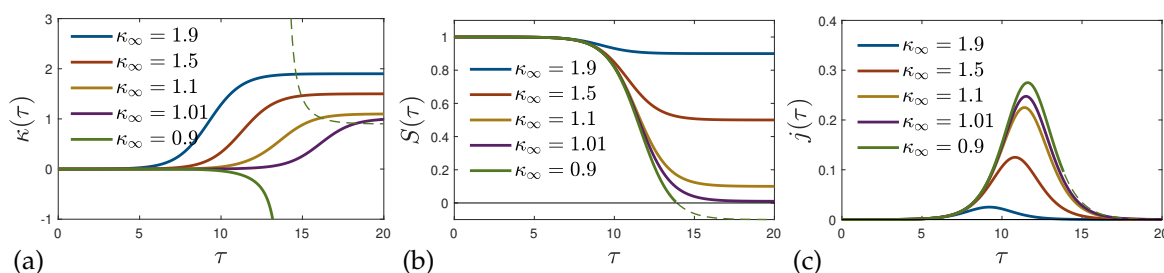


Figure 9. Analytic solution of the SIRD model for $\kappa(0) = 0$ and time-dependent $\kappa(\tau)$, parameterized by κ_∞ . (a) $\kappa(\tau)$ according to Equation (134), (b) $S(\tau)$ given by Equation (36) and (c) $j(\tau)$ from Equation (44), using τ_0 and τ_{\max} from Equations (130a) and (130b). The curves in (b) and (c) are confirmed by the numerical solution of the SIRD model. For $\kappa_\infty < K_0 \approx 1$ and $\kappa_\infty > 2K_0 \approx 2$, the analytic solution is still correct, but only useful until the pandemic has terminated, as $S(\tau)$ becomes negative (dashed lines within this regime) for $\tau > \tau_{\text{fin}}$. For the plot $\eta = 10^{-5}$.

5. Approximate Analytical Solutions of the SIRVD Model

Recently, it has been demonstrated that an accurate analytical approximation to the SIR and SIRV equations [21, 26] exists if the cumulative fraction of new infections $J(t) = J(\tau)$ at all times is much smaller than unity. For the COVID-19 outbreaks in many countries this assumption is well fulfilled.

According to Equation (19) in ref. [21] the approximation $1 - J(\tau) \simeq 1 - J_\infty$ in Equation (21) provides the solution

$$V(\tau) \simeq (1 - J_\infty) [1 - e^{-\int_0^\tau dx b(x)}], \quad (137)$$

which approaches $V_\infty = V(\infty) = 1 - J_\infty$ after infinite time. With this result in the same limit $J \leq J_\infty \ll 1$ Equation (25) with the initial condition $j(0) = \eta(1 - \eta)$ integrates

$$\begin{aligned} j(\tau) &\simeq \eta(1 - \eta) \exp \int_0^\tau dx \left[(1 - J_\infty) e^{-\int_0^x dy b(y)} - \kappa(x) - q(x) - b(x) \right] \\ &\simeq \eta(1 - \eta) \exp \int_0^\tau dx \left[e^{-\int_0^x dy b(y)} - k(x) - q(x) - b(x) \right], \end{aligned} \quad (138)$$

where the last approximation holds due to the adopted smallness $J_\infty \ll 1$. But we keep the J_∞ in the solution (137) in order not to violate the restriction $J(\tau) + V(\tau) \leq J_\infty + V_\infty \leq 1$. By integrating Equation (138) the corresponding cumulative fraction is given by

$$J(\tau) \simeq \eta + \eta(1-\eta) \int_0^\tau dz \exp \left[\int_0^z dx (e^{-\int_0^x dy b(y)} - k(x) - q(x) - b(x)) \right]. \quad (139)$$

Likewise Equations (15) and (17)–(19) provide the approximations

$$I(\tau) \simeq \frac{j(\tau)}{1 - J_\infty - V(\tau)} = \frac{\eta(1-\eta)}{1 - J_\infty} \exp \int_0^\tau dx \left[e^{-\int_0^x dy b(y)} - k(x) - q(x) \right] = j(\tau) e^{\int_0^\tau dx b(x)}, \quad (140)$$

$$R(\tau) \simeq \int_0^\tau dx \frac{k(x)j(x)}{1 - J_\infty - V(x)} = \frac{\eta(1-\eta)}{1 - J_\infty} \int_0^\tau dz k(z) \exp \int_0^z dx \left[e^{-\int_0^x dy b(y)} - k(x) - q(x) \right], \quad (141)$$

$$D(\tau) \simeq \int_0^\tau dx \frac{q(x)j(x)}{1 - J_\infty - V(x)} = \frac{\eta(1-\eta)}{1 - J_\infty} \int_0^\tau dz q(z) \exp \int_0^z dx \left[e^{-\int_0^x dy b(y)} - k(x) - q(x) \right], \quad (142)$$

and

$$\begin{aligned} d(\tau) &= \frac{dD(\tau)}{d\tau} = q(\tau)I(\tau) = \frac{q(\tau)j(\tau)}{1 - J_\infty - V(\tau)} \\ &\simeq \frac{\eta(1-\eta)}{1 - J_\infty} q(\tau) \exp \int_0^\tau dx \left[e^{-\int_0^x dy b(y)} - k(x) - q(x) \right]. \end{aligned} \quad (143)$$

5.1. Difference between the SIRVD Death Rate and the A-Posteriori Death Rate

As it marks the difference of the death rate (143) in the SIRVD model to the a-posteriori death rate $d_{a\text{-pos}}(\tau) = q(\tau)j(\tau)$ (34) we consider first the ratio

$$\frac{d_{a\text{-pos}}(\tau)}{d(\tau)} = \frac{j(\tau)}{I(\tau)} = S(\tau) \simeq 1 - J_\infty - V(\tau) = (1 - J_\infty) e^{-\int_0^\tau dx b(x)}. \quad (144)$$

For the SIRD model with negligible vaccinations ($b(\tau) = 0$), the ratio (144) is independent of reduced time and practically equals unity as $J_\infty \ll 1$. However, for the SIRVD model including vaccinations the ratio (144) depends on time. The SIRVD death rate has a flatter τ -dependence than the a-posteriori death rate.

5.2. Conditions for Extrema

As before [21] it is straightforward to calculate the first and second time derivatives of the approximative solution (138) as

$$\begin{aligned} \frac{dj}{d\tau} &= \eta(1-\eta) \left[e^{-\int_0^\tau dy b(y)} - k(\tau) - b(\tau) - q(\tau) \right] \times \\ &\quad \exp \int_0^\tau dx \left[e^{-\int_0^x dy b(y)} - k(x) - b(x) - q(x) \right], \end{aligned} \quad (145a)$$

$$\begin{aligned} \frac{d^2j}{d\tau^2} &= \eta(1-\eta) \left(\left[e^{-\int_0^\tau dy b(y)} - k(\tau) - b(\tau) - q(\tau) \right]^2 - \frac{dk}{d\tau} - \frac{db}{d\tau} - \frac{dq}{d\tau} - b(\tau) e^{-\int_0^\tau dy b(y)} \right) \times \\ &\quad \exp \int_0^\tau dx \left[e^{-\int_0^x dy b(y)} - k(x) - b(x) - q(x) \right]. \end{aligned} \quad (145b)$$

Consequently, extrema of the rate of new infections occur at reduced times τ_E determined by

$$k(\tau_E) + b(\tau_E) + q(\tau_E) = e^{-\int_0^{\tau_E} dy b(y)} \leq 1, \quad (146)$$

where we indicate that the right-hand-side of this Equation is smaller than or equal to unity. Hence no extrema of infections occur for a sum of variations

$$k(\tau) + b(\tau) + q(\tau_E) > 1. \quad (147)$$

In the alternative case of reduced time intervals, where

$$k(\tau) + b(\tau) + q(\tau_E) < 1, \quad (148)$$

extrema are possible. From Equation (145b) one obtains

$$\begin{aligned} \left[\frac{d^2j}{d\tau^2}\right]_{\tau_E} = & -\eta(1-\eta)\left(\left[\frac{dk}{d\tau}\right]_{\tau_E} + \left[\frac{db}{d\tau}\right]_{\tau_E} + \left[\frac{dq}{d\tau}\right]_{\tau_E} + b^2(\tau_E) + b(\tau_E)k(\tau_E) + b(\tau_E)q(\tau_E)\right) \times \\ & \exp\left[\int_0^{\tau_E} dx \left(e^{-\int_0^x dy b(y)} - k(x) - b(x) - q(x)\right)\right], \end{aligned} \quad (149)$$

Hence, the extrema are maxima if

$$\left[\frac{dk}{d\tau}\right]_{\tau_E} + \left[\frac{db}{d\tau}\right]_{\tau_E} + \left[\frac{dq}{d\tau}\right]_{\tau_E} + b^2(\tau_E) + b(\tau_E)k(\tau_E) + b(\tau_E)q(\tau_E) > 0 \quad (150)$$

is positive. They are minima if

$$\left[\frac{dk}{d\tau}\right]_{\tau_E} + \left[\frac{db}{d\tau}\right]_{\tau_E} + \left[\frac{dq}{d\tau}\right]_{\tau_E} + b^2(\tau_E) + b(\tau_E)k(\tau_E) + b(\tau_E)q(\tau_E) < 0 \quad (151)$$

is negative. There can be multiple minima and maxima depending on the reduced time variation of the ratios $k(\tau)$ and $b(\tau)$. The extreme values of the rate of new infections are given by

$$j_E(\tau_E) = \eta(1-\eta)e^{\int_0^{\tau_E} dx \left[e^{-\int_0^x dy b(y)} - k(x) - b(x) - q(x)\right]}. \quad (152)$$

All results given in this Section for the SIRVD model include as special cases the corresponding quantities in the SIRD model for $b(\tau) = 0$ and the SIR model for $b(\tau) = q(\tau) = 0$, respectively. The excellent agreement with the respective numerical solutions of the SIR and SIRV models [21,26] has proven the validity of the analytical approximation using the smallness of $J(\tau) \ll 1$.

6. SIRVD Model Applications

Next we illustrate our results from the preceding section with two examples. While section 6.1 is concerned with the case of stationary ratios, in section 6.2 we work out the case of a gradually decreasing fatality rate.

6.1. Special Case: Stationary Ratios

We first consider the approximative solutions (137) and (138) in the special case of stationary ratios

$$\begin{aligned} k(\tau) &= k_0, \\ b(\tau) &= b_0, \\ q(\tau) &= q_0 \end{aligned} \quad (153)$$

This case corresponds to the numerical solutions of the SIRVD model shown before in Figure 2. If we introduce $k_0 = k_0 + b_0$ we may use the earlier results of ref.[21] to obtain

$$V(\tau) = (1 - J_\infty)[1 - e^{-b_0\tau}], \quad (154)$$

and

$$j(\tau) = \eta(1 - \eta) \exp \left[\frac{1 - e^{-b_0\tau}}{b_0} - (\kappa_0 + b_0)\tau \right]. \quad (155)$$

Provided $\kappa_0 + b_0 = k_0 + q_0 + b_0 < 1$, the rate of new infections (155) attains its maximum value

$$\begin{aligned} j_{\max} &= j(\tau_m) = \eta(1 - \eta)(\kappa_0 + b_0)^{\frac{\kappa_0 + b_0}{b_0}} e^{\frac{1 - (\kappa_0 + b_0)}{b_0}} \\ &= \eta(1 - \eta)(k_0 + q_0 + b_0)^{\frac{k_0 + q_0 + b_0}{b_0}} e^{\frac{1 - (k_0 + q_0 + b_0)}{b_0}}. \end{aligned} \quad (156)$$

at the reduced time

$$\tau_m = -\frac{\ln(k_0 + q_0 + b_0)}{b_0}. \quad (157)$$

For the cumulative fraction one finds

$$\begin{aligned} J(\tau) &= \eta + \eta(1 - \eta)b_0^{\frac{\kappa_0}{b_0}} e^{\frac{1}{b_0}} \left[\gamma \left(1 + \frac{\kappa_0}{b_0}, \frac{1}{b_0} \right) - \gamma \left(1 + \frac{\kappa_0}{b_0}, \frac{e^{-b_0\tau}}{b_0} \right) \right] \\ &= \eta + \eta(1 - \eta)b_0^{\frac{k_0 + q_0}{b_0}} e^{\frac{1}{b_0}} \left[\gamma \left(1 + \frac{k_0 + q_0}{b_0}, \frac{1}{b_0} \right) - \gamma \left(1 + \frac{k_0 + q_0}{b_0}, \frac{e^{-b_0\tau}}{b_0} \right) \right] \end{aligned} \quad (158)$$

in terms of the lower incomplete gamma function γ . For infinitely large times, the fraction (158) approaches the final value

$$J_\infty = J(\tau = \infty) = \eta + \eta(1 - \eta)b_0^{\frac{k_0 + q_0}{b_0}} e^{\frac{1}{b_0}} \gamma \left(1 + \frac{k_0 + q_0}{b_0}, \frac{1}{b_0} \right). \quad (159)$$

Likewise, the SIRVD death rate (143) in this case becomes

$$d(\tau) = \frac{dD(\tau)}{d\tau} \simeq \eta(1 - \eta)q_0 \exp \left[\frac{1 - e^{-b_0\tau}}{b_0} - (k_0 + q_0)\tau \right] = q_0 e^{b_0\tau} j(\tau) = e^{b_0\tau} d_{a\text{-pos}}(\tau). \quad (160)$$

It differs from the a-posteriori death rate by the factor $e^{b_0\tau}$ reflecting the ratio between $I(\tau)$ and $j(\tau)$. The rate (160) peaks at the time

$$\tau_d = -\frac{\ln(k_0 + q_0)}{b_0}, \quad (161)$$

which is greater than the peak time τ_m of the rate of new infections. The maximum SIRVD death rate

$$d_{\max} = q_0 \eta(1 - \eta)(k_0 + q_0)^{\frac{k_0 + q_0}{b_0}} e^{\frac{1 - k_0 - q_0}{b_0}} = \frac{e^1}{k_0 + q_0} \left[1 + \frac{b_0}{k_0 + q_0} \right]^{-[1 + \frac{k_0 + q_0}{b_0}]} d_{\max}^{\text{a-pos}} \quad (162)$$

is smaller than the maximum a-posteriori death rate.

The corresponding cumulative fraction of fatalities is given by

$$D(\tau) = q_0 \eta(1 - \eta)b_0^{\frac{k_0 + q_0 - b_0}{b_0}} e^{\frac{1}{b_0}} \left[\gamma \left(\frac{k_0 + q_0}{b_0}, \frac{1}{b_0} \right) - \gamma \left(\frac{k_0 + q_0}{b_0}, \frac{e^{-b_0\tau}}{b_0} \right) \right], \quad (163)$$

with the final value

$$D_\infty = D(\tau = \infty) = q_0 \eta(1 - \eta)b_0^{\frac{k_0 + q_0 - b_0}{b_0}} e^{\frac{1}{b_0}} \gamma \left(\frac{k_0 + q_0}{b_0}, \frac{1}{b_0} \right)$$

$$= \frac{q_0 \eta (1 - \eta)}{k_0 + q_0} \left[b_0^{\frac{k_0 + q_0}{b_0}} e^{\frac{1}{b_0}} \gamma \left(1 + \frac{k_0 + q_0}{b_0}, \frac{1}{b_0} \right) + 1 \right]. \quad (164)$$

It has been shown before in Equation (57) of ref. [21] that for small values of $b_0 \ll 1$ and $b_0 < \kappa_0 = k_0 + q_0 < 1$ the cumulative fractions as well as their final values have to be calculated with the leading order approximation for large values of $z \gg 1$

$$z^{-\kappa_0 z} \gamma(1 + \kappa_0 z, z) \simeq \sqrt{2\pi \kappa_0 z} \kappa_0^{\kappa_0 z - 1} e^{-\kappa_0 z} - 1. \quad (165)$$

Applying this approximation to Equations (159) and (164) with $z = b_0^{-1}$ provides

$$J_\infty \simeq \eta(1 - \eta) \left[\sqrt{\frac{2\pi(k_0 + q_0)}{b_0}} e^{\frac{1 - (k_0 + q_0)}{b_0}} (k_0 + q_0)^{\frac{k_0 + q_0}{b_0} - 1} - 1 \right], \quad (166a)$$

$$D_\infty \simeq \frac{q_0 \eta (1 - \eta)}{k_0 + q_0} \sqrt{\frac{2\pi(k_0 + q_0)}{b_0}} e^{\frac{1 - (k_0 + q_0)}{b_0}} (k_0 + q_0)^{\frac{k_0 + q_0}{b_0} - 1} \simeq \frac{1}{k_0 + q_0} D_\infty^{\text{a-pos}}. \quad (166b)$$

We note that the ratio $D_\infty / D_\infty^{\text{a-pos}}$ does not depend on the value of b_0 .

These differences are clearly seen in the panels of Figure 10. The SIR, SIRV and SIRD curves, representing a-posteriori death rates, have a significant different reduced time dependence compared to the SIRVD curve. For the values of $k_0 = 0.5$, $b_0 = 0.1$ and $q_0 = 0.1$ shown in Figure 10-a,b, the maximum death rate is a factor 1.54 smaller than the maximum a-posteriori death rate, the final cumulative fraction of fatalities is a factor 1.67 larger than its a-posteriori value, and the death rate peaks at the earlier time $\tau_d = 5.1$ as compared to $\tau_m = 3.6$. The performance of the analytical solution $j(\tau)$ (155) of the SIRVD model over a wide range of its determining parameters κ_0 and b_0 is analyzed in Figure 11.

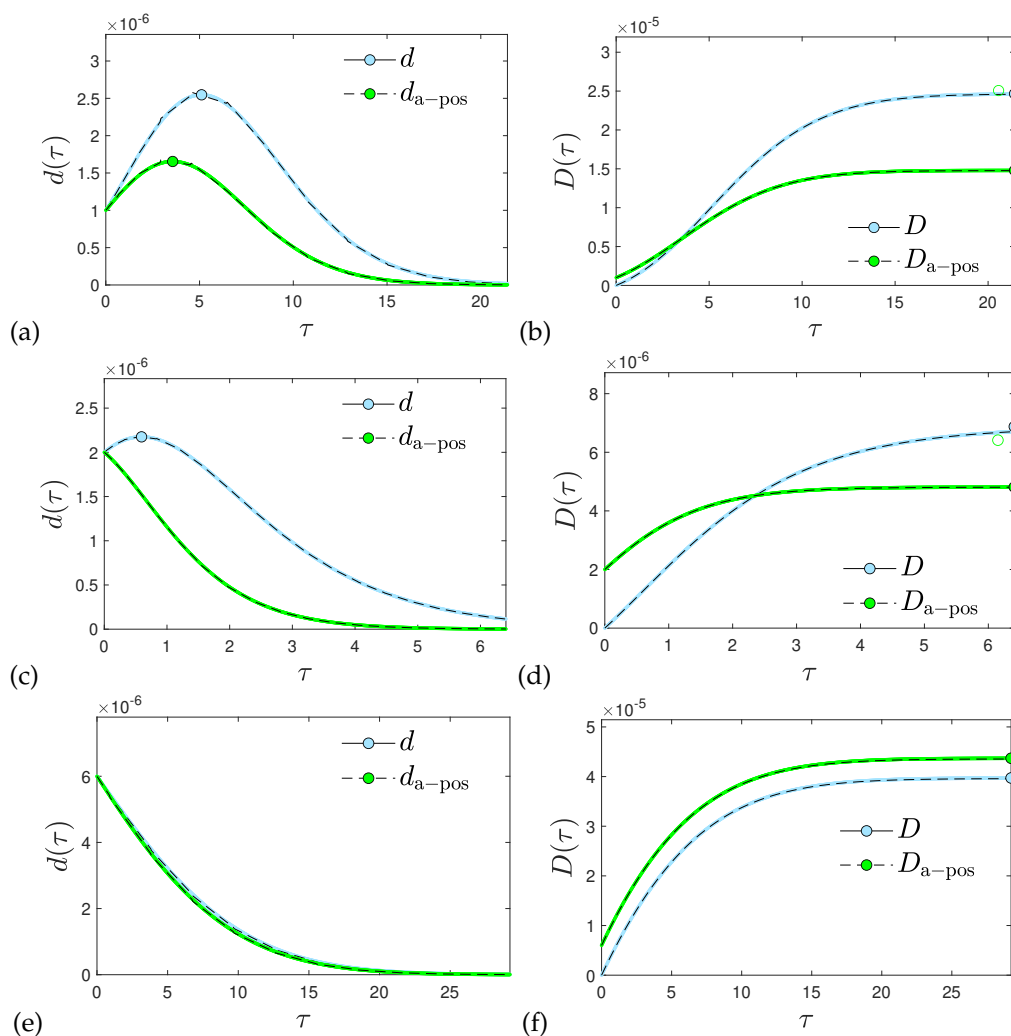


Figure 10. Analytical (solid colored) and numerical solutions (dashed black) of the SIRVD model at $\eta = 10^{-5}$ and (a,b) $k_0 = 0.5, q_0 = 0.1, b_0 = 0.1$, (c,d) $k_0 = 0.5, q_0 = 0.2, b_0 = 0.6$, (e,f) $k_0 = 0.5, q_0 = 0.6, b_0 = 0.01$. (a,c,e) $d(\tau)$ as well as $d_{a\text{-pos}}(\tau)$ according to Equation (160). The bullets are located at (τ_d, d_{\max}) (blue) and $(\tau_m, q_0 j_{\max})$ (green), given by Equations (161), (162), (156), and (157). (b,d,f) $D(\tau)$ as well as $D_{a\text{-pos}}(\tau) = q_0 J(\tau)$, using Equations (158), (163). The bullets mark the final values D_∞ (blue) and $D_\infty^{a\text{-pos}}$ (green) according to Equation (164); open bullets for the approximant (166b).

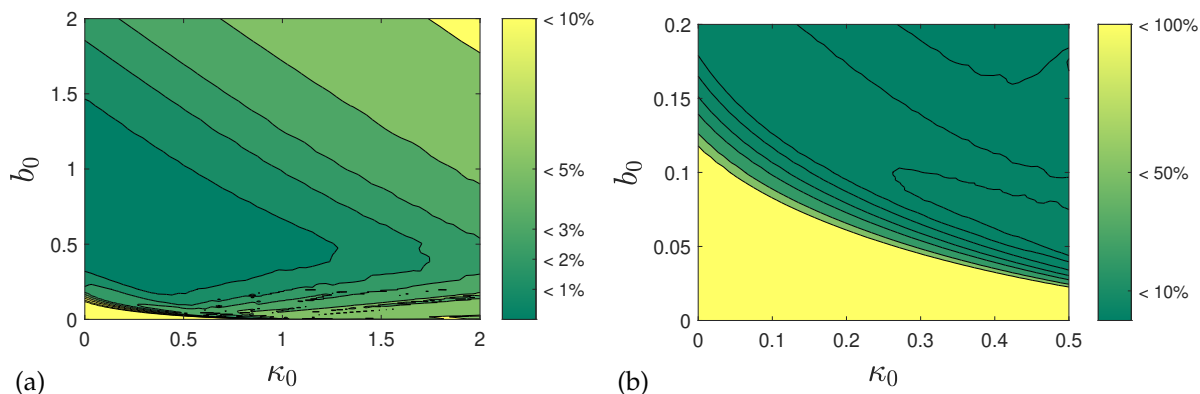


Figure 11. Performance of the analytic solution of the SIRVD model for $\eta = 10^{-5}$ and constant rates in κ_0 - b_0 space. Shown is the mean percentage of deviation between the analytic $j(\tau)$ from Equation (155), and the numerical solution. The plot looks nearly identical for all remaining differential and cumulative quantities, including $d(\tau)$ and $D(\tau)$ from Equations (160) and (163), for any k_0 (or q_0). (a) shows the range $\kappa_0, b_0 \in [0, 2]$, while (b) offers a zoom into the bottom left region $\kappa_0 \in [0, 0.5]$ and $b_0 \in [0, 0.2]$ of pronounced relative deviations, while the absolute deviation is still small, as visible from Figure 10-e,f, where we show a case that resides in the yellow region.

6.2. Gradually Decreasing Fatality Rate

Here we use the approximative solutions (137) and (138) in the special case of stationary ratios $K(\tau) = k_0, b(\tau) = b_0$ but the gradually decreasing fatality rate

$$q(\tau) = q_0 - q_1(1 - e^{-G\tau}) \quad (167)$$

with constants q_0, q_1 and G . The fatality rate (168) starts from the constant value q_0 and decreases with the typical time scale G^{-1} to its final constant value q_1 . Such a behavior accounts well for the COVID-19 omicron which had a much smaller (about an order of magnitude) fatality rate than the earlier mutants [22] occurring about a year earlier. Such a slow gradual decrease is well captured by the adopted fatality rate (168) in the case $G \ll b_0 < 1$, allowing us the linear approximation

$$q(\tau \leq G^{-1}) \simeq q_0 - q_1 G \tau, \quad (168)$$

if necessary.

The vaccination rate (154) is independent from the fatality rate $q(\tau)$ and also here, whereas with the rate (167) the rate of new infections (138) becomes

$$j(\tau) \simeq \eta(1 - \eta) \exp \left[\frac{1 - e^{-b_0\tau}}{b_0} - (k_0 + b_0 + q_0 - q_1)\tau - q_1 \frac{1 - e^{-G\tau}}{G} \right]. \quad (169)$$

Consequently, one finds for Equations (140)–(143)

$$I(\tau) = j(\tau)e^{b_0\tau} \simeq \eta(1 - \eta) \exp \left[\frac{1 - e^{-b_0\tau}}{b_0} - (k_0 + q_0 - q_1)\tau - q_1 \frac{1 - e^{-G\tau}}{G} \right], \quad (170a)$$

$$R(\tau) \simeq k_0 I(\tau) = \eta(1 - \eta)k_0 \exp \left[\frac{1 - e^{-b_0\tau}}{b_0} - (k_0 + q_0 - q_1)\tau - q_1 \frac{1 - e^{-G\tau}}{G} \right], \quad (170b)$$

$$d(\tau) = [q_0 - q_1(1 - e^{-G\tau})]\eta(1 - \eta) \exp \left[\frac{1 - e^{-b_0\tau}}{b_0} - (k_0 + q_0 - q_1)\tau - q_1 \frac{1 - e^{-G\tau}}{G} \right] \quad (170c)$$

and

$$D(\tau) \simeq \eta(1 - \eta) \int_0^\tau dz [q_0 - q_1(1 - e^{-Gz})] \exp \left[\frac{1 - e^{-b_0z}}{b_0} - (k_0 + q_0 - q_1)z - q_1 \frac{1 - e^{-Gz}}{G} \right], \quad (171)$$

respectively, whereas the cumulative fraction of infections is given by

$$J(\tau) \simeq \eta + \eta(1 - \eta) \int_0^\tau dz \exp \left[\frac{1 - e^{-b_0z}}{b_0} - (k_0 + b_0 + q_0 - q_1)z - q_1 \frac{1 - e^{-Gz}}{G} \right]. \quad (172)$$

The analytical expressions are in excellent agreement with the numerical solutions of the SIRVD model in the presence of time-dependent $q(\tau)$. In Figure 13 we show selected results for $j(\tau)$ and $d(\tau)$, while all other quantities are equally well captured.

6.2.1. Peak Times

For values of $k_0 + b_0 + q_0 < 1$ the rate of new infections (169) peaks at the time given by

$$e^{-b_0\tau_m} - q_1 e^{-G\tau_m} = k_0 + b_0 + q_0 - q_1, \quad (173)$$

whereas the death rate (170c) attains its maximum at τ_d determined by

$$[q_0 - q_1(1 - e^{-G\tau_d})][e^{-b_0\tau_d} - k_0] - q_1(G + 2q_0 - 2q_1)e^{-G\tau_d} - (q_0 - q_1)^2 - q_1^2 e^{-2G\tau_d} = 0 \quad (174)$$

Both Equations (173)–(174) are nonlinear and cannot be solved in closed form². However, if we use, as in Equation (168), the approximation $e^{-G\tau_{m,d}} \simeq 1 - G\tau_{m,d}$ Equations (173)–(174) can be approximated as

$$e^{-b_0\tau_m} \simeq -q_1 G\tau_m + C_0, \quad C_0 = k_0 + b_0 + q_0, \quad (175)$$

and

$$(q_0 - q_1 G\tau_d) e^{-b_0\tau_d} = q_0(k_0 + q_0) + q_1 G - q_1 G(k_0 + 2q_0 + G)\tau_d. \quad (176)$$

This latter equation (176), treated below, is of the form of Wright's transcendental equation. It is easy to see that Equations (169)–(176) in the limit $q_1 = 0$ correctly reduce to the earlier results in Section 6.1. The applicability of Equations (175) and (176) requires $G \ll b_0$. Introducing the positive $z_m = b_0\tau_m$ and the positive combination $a_m = b_0 C_0 / q_1 G$ of parameters, the first Equation (175) reads $e^{-z_m} = C_0(1 - z_m/a_m)$ and thus determines z_m in terms of a_m and C_0 . This latter equation is solved in terms of the non-principal Lambert function W_{-1} (see Appendix G in ref. [28]) as

$$z_m = a_m + W_0 \left(-\frac{e^{-1/a_m}}{a_m C_0} \right), \quad \tau_m = \frac{C_0}{q_1 G} + \frac{1}{b_0} W_{-1} \left(-\frac{b_0 e^{-b_0 C_0 / q_1 G}}{q_1 G} \right), \quad (177)$$

where we have just re-inserted z_m and a_m in the second part of Equation (177).

As detailed in Appendix C the solution of Equation (176) is more involved. As for the calculation of τ_m , it is helpful to introduce a dimensionless time $z_d = b_0\tau_d$, and to simplify Equation (176) using an appropriate combination of the five semipositive parameters k_0 , b_0 , q_0 , q_1 , G , and z_d . As shown in Appendix C it is possible to write Equation (176) in the form of Wright's transcendental equation,

$$e^{-X} = 1 - \frac{2b}{b - a - X}, \quad (178)$$

² This is known from the works of Évariste Galois who died during a duel at the age of 20 in 1832. His important contribution, known as Galois theory, was recognized and published 14 years later by Joseph Liouville [27].

or equivalently

$$a = -X - b \coth(X/2) \quad (179)$$

upon introducing X , a , and b via

$$\begin{aligned} X &= z_d + \ln C_1, & C_1 &= k_0 + 2q_0 + G, \\ a &= b - \frac{b_0 q_0}{q_1 G} - \ln C_1, \\ b &= \frac{q_0 + (1 - q_1/q_0)G}{2C_1} \frac{b_0 q_0}{q_1 G}, \end{aligned} \quad (180)$$

Since $q_1 < q_0$ to ensure positive $q(\tau)$, one has $b > 0$. Further, $a < 0$ since $G \ll b_0$. For positive values of b and negative values of a , no solutions to Equation (179) with negative X are possible. This is most easily seen by rewriting this equation as $a + X = b \coth(X/2)$. For negative X , the right hand side is negative, while left hand side is positive. Equation (179) hence implies $X > 0$, and $z_d > 0$ implies $X > \ln C_1$. The equation (178) is equivalent to Wright's transcendental equation and known [29] to exhibit real-valued solutions X only for a limited range of a and b values. Using the x -parametric form of the envelope $a = -x - \sinh(x)$ and $b = -1 + \cosh(x)$ [29] we derive the condition

$$a \leq -\sqrt{b}\sqrt{2+b} - \cosh^{-1}(1+b) \equiv a_{\max} \leq 0 \quad (181)$$

for the existence of a τ_d value. The a_{\max} monotonically decreases with increasing b , starting from $a_{\max} = 0$ and $b = 0$.

In Appendix C we obtain the following approximations for the exact solution of Equation (179):

$$X_0 \simeq \frac{b-a}{2} \left[1 - \sqrt{1 - \frac{8b}{(b-a)^2}} \right] \simeq \frac{2b}{b-a}, \quad (X \in [0, 1]) \quad (182a)$$

$$X_1 \simeq -\frac{3a + \sqrt{9a^2 - 12b(6+b)}}{6+b} \quad (X \in [0, 2], a < -\frac{2\sqrt{b(6+b)}}{\sqrt{3}}), \quad (182b)$$

$$X_2 \simeq \frac{a^2 - b^2}{2b} + W_{-1} \left(-\frac{(a-b)^2 e^{-(a^2-b^2)/2b}}{2b} \right), \quad (X < b-a) \quad (182c)$$

Note that X_0 approaches unity for $a = a_{\max}$ and $b \rightarrow \infty$, while $X_2 \rightarrow \infty$ behaves correctly in this limit. As detailed in Appendix C, X_0 is most precise for sufficiently small a well below a_{\max} , X_1 performs extremely well (Figure 12) over the whole a - b range except very close to $a = a_{\max}$ and large b , while X_2 has advantages only in the regime where X_1 fails. To summarize, τ_d exists as long as $a < a_{\max}$, and is then well approximated by

$$\tau_d \simeq \frac{X_1 - \ln(k_0 + 2q_0 + G)}{b_0} \quad (183)$$

with a and b expressed in terms of k_0 , b_0 , q_0 , q_1 , and G via Equation (180). In Figure 13 we mark the analytical τ_m and τ_d for a few cases. As visible, they capture the peak times of the analytical solutions for $j(\tau)$ (169) and $d(\tau)$ (170c), that moreover are indistinguishable from the numerical solution. Since it is impossible to visualize the performance of the numerical versus analytical results for the case of time-dependent $q(\tau)$, characterized by 6 parameters k_0 , b_0 , q_0 , q_1 , G , and η , we have randomly chosen sets of parameters with $k_0, q_0, b_0 \in [0, 1]$, $q_1 \in [0, q_0]$, $G \in [0, b_0]$, and $\eta \in [10^{-7}, 10^{-3}]$. The comparison is undertaken in Figure 14.

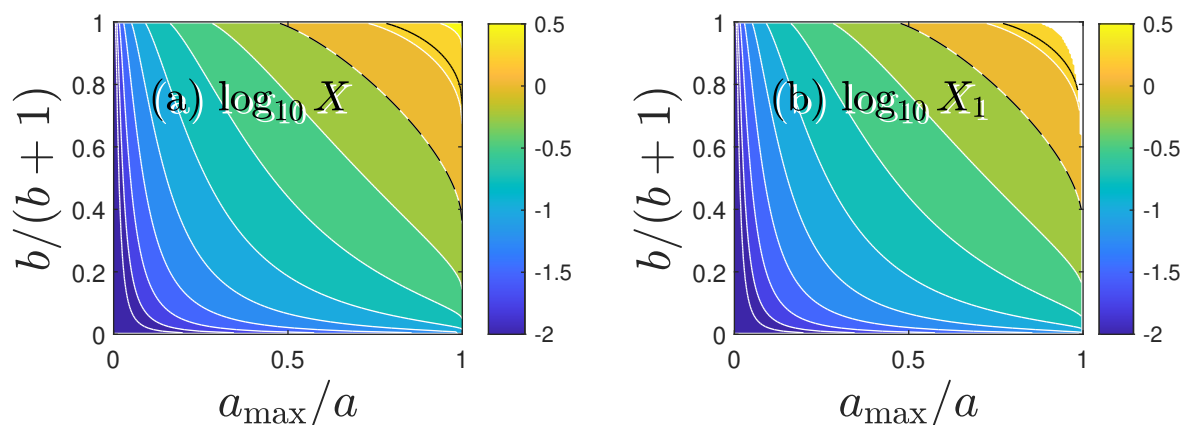


Figure 12. (a) The exact solution X to Equation (178) or (179) versus a_{\max}/a and $b/(b+1)$ with the negative a_{\max} defined by Equation (181). (b) Approximant X_1 given by Equation (182b). It is undefined in the small white region in the top right corner, characterized by $a < -2\sqrt{b(6+b)}/3$. Two contourlines are highlighted in each panel: $X = 1$ (dashed black) and $X = 2$ (solid black). For the remaining approximants X_0 and X_2 see Figure A1 in Appendix C.

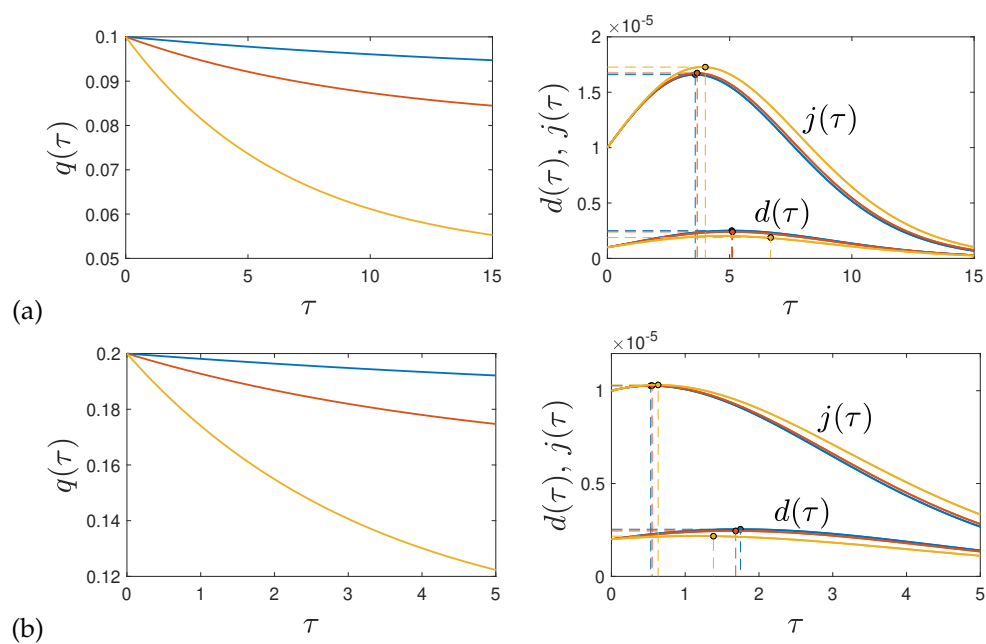


Figure 13. SIRVD model at time-dependent $q(\tau) = q_0 - q_1(1 - e^{-G\tau})$. Analytic $d(\tau)$ and $j(\tau)$ coincide basically exactly with the numerical solution. Highlighted are the analytic position and height of the maxima, (τ_m, j_{\max}) , Equations (177), (184) and (τ_d, d_{\max}) , Equations (183), (185). Parameters: (a) $k_0 = 0.5, q_0 = 0.1, b_0 = 0.1, \eta = 10^{-5}$ and (b) $k_0 = 0.5, q_0 = 0.2, b_0 = 0.2, \eta = 10^{-5}$. In (a,b) the three colors represent $G = 0.5b_0, q_1 = 0.1q_0$ (blue), $G = b_0, q_1 = 0.2q_0$ (red), $G = 1.5b_0, q_1 = 0.5q_0$ (yellow).

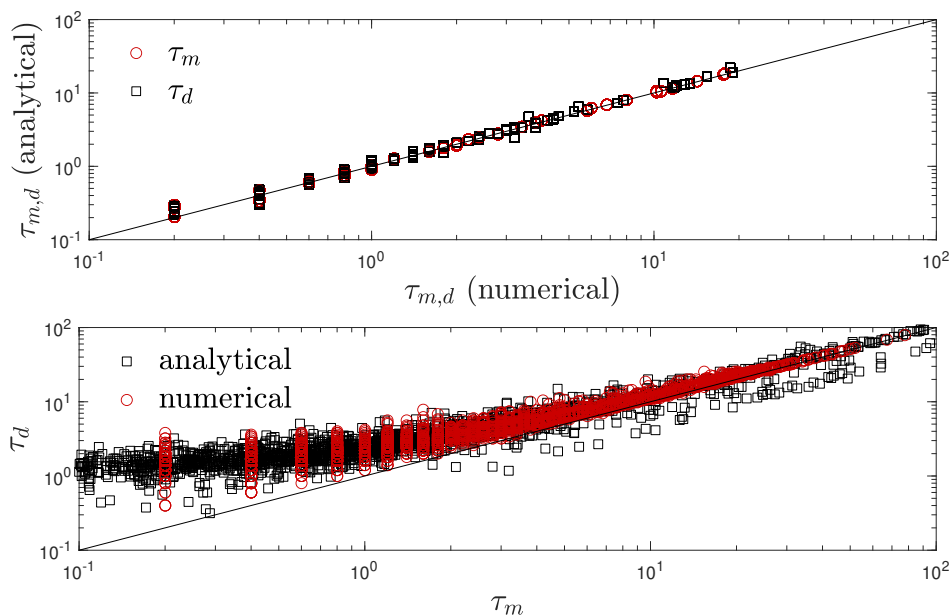


Figure 14. Since it is impossible to visualize the performance of the numerical versus analytical results for the case of time-dependent $q(\tau)$, characterized by 6 parameters k_0, b_0, q_0, q_1, G , and η , we have randomly chosen sets of parameters with $k_0, q_0, b_0 \in [0, 1], q_1 \in [0, q_1], G \in [0, b_0]$, and $\eta \in [10^{-7}, 10^{-3}]$. The number of sets is (a) 100 and (b) 5000. In (a) we visualize the performance of analytical versus numerical results for τ_m (177) and τ_d (183), while (b) shows τ_d versus τ_m , both numerical value (red circles) and analytical expressions (black squares). The numerical results suggest $\tau_d \geq \tau_m$, while this is not reflected by 1.5% of the analytical results.

6.2.2. Maximum Rate of New Infections and Death Rate

With the peak times (177) and (183) inserted in Equations (169) and (170c), respectively, the maximum rates of the new infections and the maximum death rates are given by

$$\begin{aligned}
 j_{\max} &= \eta(1-\eta)e^{\frac{1-k_0-b_0-q_0+q_1}{b_0}-\frac{q_1}{G}} \exp\left[\frac{q_1(b_0-G)}{b_0G}e^{-G\tau_m} - (k_0+b_0+q_0-q_1)\tau_m\right] \\
 &\simeq \eta(1-\eta)e^{\frac{1-k_0-b_0-q_0+q_1}{b_0}-\frac{q_1}{G}} \exp\left[\frac{q_1(b_0-G)}{b_0G}e^{-\frac{k_0+b_0+q_0}{q_1}-\frac{G}{b_0}W_{-1}\left(-\frac{b_0e^{-b_0(k_0+b_0+q_0)}/q_1G}{q_1G}\right)}\right. \\
 &\quad \left. - (k_0+b_0+q_0-q_1)\left[\frac{k_0+b_0+q_0}{q_1} + \frac{1}{b_0}W_{-1}\left(-\frac{b_0e^{-b_0(k_0+b_0+q_0)}/q_1G}{q_1G}\right)\right]\right], \quad (184)
 \end{aligned}$$

where we made use of the determining Equation (173), and

$$\begin{aligned}
 d_{\max} &= [q_0 - q_1(1 - e^{-G\tau_d})]\eta(1-\eta)e^{\frac{1}{b_0}-\frac{q_1}{G}} \exp\left[-\frac{e^{-b_0\tau_d}}{b_0} - (k_0+q_0-q_1)\tau_d + \frac{q_1e^{-G\tau_d}}{G}\right] \\
 &= [q_0 - q_1(1 - (k_0 + 2q_0 + G)^{\frac{G}{b_0}}e^{-\frac{GX_1}{b_0}})]\eta(1-\eta)e^{\frac{1}{b_0}-\frac{q_1}{G}} \exp\left[-\frac{(k_0 + 2q_0 + G)e^{-X_1}}{b_0}\right. \\
 &\quad \left. - \frac{k_0 + q_0 - q_1}{b_0}(X_1 - \ln(k_0 + 2q_0 + G)) + \frac{q_1}{G}(k_0 + 2q_0 + G)^{\frac{G}{b_0}}e^{-\frac{GX_1}{b_0}}\right]. \quad (185)
 \end{aligned}$$

6.2.3. Death Rates

In Figure 15 we compare the death rate (170c) and the a-posteriori death rate (34)

$$d_{a\text{-pos}}(\tau) = [q_0 - q_1(1 - e^{-G\tau})]j(\tau) \quad (186)$$

with $j(\tau)$ from Equation (169) for six different choices of parameters. In each case the analytical death rates agree very well with the corresponding numerical solutions of the SIRVD model proving the accuracy of the analytical approximation.

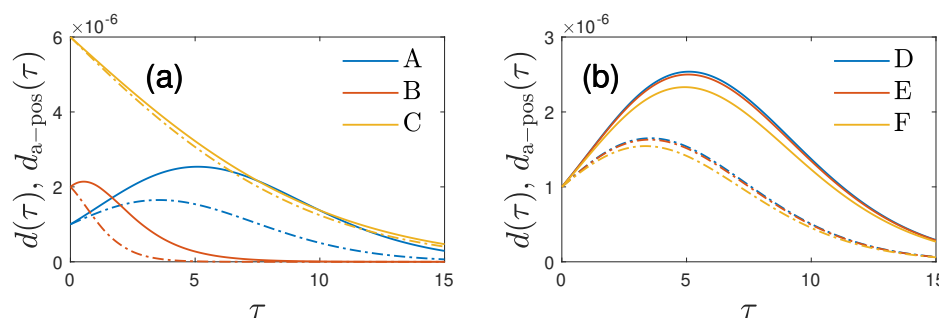


Figure 15. Comparison between death rate $d(\tau)$ (solid line), Equation (170c), and a-posteriori death rate $d_{a\text{-pos}}(\tau)$ (dot-dashed), Equation (186), for the SIRVD model with gradually decreasing $q(\tau)$. In (a) and (b) the following six cases are shown: (A) $q_0 = 0.1, b_0 = 0.1, q_1 = 0.1q_0, G = 0.1b_0$, (B) $q_0 = 0.2, b_0 = 0.6, q_1 = 0.5q_0, G = 0.1b_0$, (C) $q_0 = 0.6, b_0 = 0.01, q_1 = 0.5q_0, G = 0.1b_0$, (D,E,F) same q_0 and b_0 as in (A) but different q_1 and G : (D) $q_1 = 0.1q_0, G = 0.1b_0$, (E) $q_1 = 0.5q_0, G = 0.1b_0$, (F) $q_1 = 0.5q_0, G = 0.5b_0$. In each case $k_0 = 0.5$ and $\eta = 10^{-5}$. The analytic results coincide with the numerical results within $< 1\%$ relative deviation.

We observe earlier peak-times for the a-posteriori death rates, following the rate $j(\tau)$ of newly infected individuals, compared with the SIRVD death rate $d(\tau)$, following $I(\tau)$. Additionally, the SIRVD death rates are significantly larger compared with those obtained through the a-posteriori treatment, with direct implications for the corresponding D_∞ values. Our predictions for these differences are suitable for being corroborated with past monitored pandemic data on the rate of new infections and the death rates of sufficient quality with negligible underestimation i.e. negligible dark numbers.

7. Summary and Conclusions

We have investigated a special class of exact solutions as well as accurate analytical approximations of the SIRVD and SIRD compartment models. For nonlinear models with a high-dimensional parameter space analytical solutions, exact or accurately approximative, are of high importance and interest: not only as suitable benchmarks for numerical codes, but especially as they allow us to understand the critical behavior of epidemic outbursts as well as the decisive role of certain parameters [30]. For given reduced time variations of the ratios $k(\tau)$, $q(\tau)$ and $b(\tau)$ the SIRVD and SIRD equations represent complicated integro-differential equations for the rate of new infections $j(\tau)$ as well as the cumulative fraction of infections $J(\tau)$, or $S(\tau)$ and $I(\tau)$. However, the integro-differential equations can also be regarded as simpler determining equations for the sum of ratios $k(\tau) + q(\tau) = \kappa(\tau)$ for given variations of the ratio $b(\tau)$ and the fraction $S(\tau)$. This new approach has been used to derive fully exact analytical solutions for the SIRVD and SIRD models. Especially for the SIRD model it is an effective new method to construct a special class of exact solutions depending on two parameters which are chosen as the values of the ratio $\kappa(\tau)$ at the start ($\kappa(\tau = 0)$) and the end ($\kappa(\tau = \infty)$) of the epidemic outburst. The new method for the SIRD case is illustrated in Section 4 for three different choices of the two parameters including a detailed investigation of the properties of the constructed solutions. Particular interesting are the cases where the combined ratio $\kappa(\tau)$ at the start and the end of the epidemic outburst have values below $K \leq 0.5$ which corresponds to infection rates being twice as large as the sum of the recovery and fatality rate. In this case the epidemic outburst, described by the SI-type $\cosh^{-2}[(\tau - \tau_{\max})/\tau_0]$ -distribution for the rate of new infections, is so dominated by the rapid infections that at the finite reduced time τ_{fin} the outburst suddenly terminates as with $S(\tau_{\text{fin}}) = 0$ no more persons are available to be infected. The situation is

comparable to a smooth running car where suddenly the car engine stops as no more fuel is available. For values greater than $K > 0.5$ the epidemic outburst lasts until infinitely large times.

In the second part of the manuscript the recently developed analytical approximation [20,21] for the SIR and SIRV models are applied to the more general SIRVD model. In the limit of small cumulative fractions $J \ll 1$, which very often is fulfilled, this approximation provides accurate analytical expressions for all epidemic quantities of interest such as the rate of new infections $\dot{J}(t)$ and the fraction $I(t)$ of infected persons. As an aside, when determining τ_d in Appendix C we provided accurate approximative solutions to Wright's transcendental equation (A16), or equivalently, Equation (178). The main difference of the SIRVD to the SIRV model is the discrimination between recovered and deceased persons by introducing two different compartments which affects the calculation of the death rate. In the SIRVD/SIRD cases it is proportional to $I(t)$, whereas in many SIR models in an a-posteriori approach it is proportional to $\dot{J}(t)$. It is shown that the temporal dependence of $I(t)$ and $\dot{J}(t)$ are different when the effect of vaccinations is included and/or when the real time dependence of the fatality rate $\psi(t)$ and the recovery rate $\mu(t)$ are different from each other. We illustrate these pronounced differences with two applications: one for stationary ratios k_0, b_0 and q_0 , and one for stationary ratios k_0, b_0 but a gradually decreasing fatality rate. In our analysis, we observe earlier peak-times for the rate of newly infected individuals compared with death rates. Additionally, our findings indicate significantly smaller death rates compared with those obtained through the a-posteriori treatment. We are hopeful that these differences can be corroborated with past monitored pandemic data on the rate of new infections and the death rates of sufficient quality, with negligible underestimation. We didn't account for the widely acknowledged 7-day delay between the onset of infection and the resulting death. This delay impacts both the death rate in our SIRVD model and the subsequent a-posteriori death rate analysis in a consistent manner. As a result, the derived difference in peak times remains unchanged.

Author Contributions: Conceptualization, R.S.; Methodology, R.S. and M.K.; Formal analysis, M.K. and R.S.; Writing—original draft, R.S.; Writing—review & editing, M.K.; Visualization, M.K.. All authors have read and agreed to the published version of the manuscript.

Funding: This research received no external funding.

Data Availability Statement: All data are enclosed with this publication.

Acknowledgments: We acknowledge support by chatgpt in rephrasing the abstract, and removing all mathematical symbols from our version.

Conflicts of Interest: The authors declare no conflicts of interest.

Appendix A. SI Model

In the case of vanishing $k(\tau) = q(\tau) = b(\tau) = 0$ the SIRVD equations (11a)–(11f) reduce to

$$\frac{dS}{d\tau} = -SI, \quad (\text{A1a})$$

$$\frac{dI}{d\tau} = SI, \quad (\text{A1b})$$

$$1 = S(\tau) + I(\tau), \quad (\text{A1c})$$

subject to initial conditions $I(0) = \eta = 1 - S(0)$. Equation (A1b) provides $S = d \ln I / d\tau$, so that the sum constraint (A1c) reads

$$\frac{dI(\tau)}{d\tau} = I(\tau) - I^2(\tau). \quad (\text{A2})$$

Equation (A2) leads to the integral

$$\tau = \int_{\eta}^I \frac{dz}{z - z^2} = \int_{\frac{1}{I}}^{\frac{1}{\eta}} \frac{dy}{y - 1} = \ln \frac{\frac{1}{\eta} - 1}{\frac{1}{I} - 1}, \quad (\text{A3})$$

where we substituted $z = 1/y$. Equation (A3) provides

$$I(\tau) = \frac{1}{1 + \frac{1-\eta}{\eta} e^{-\tau}} \quad (\text{A4a})$$

$$S(\tau) = 1 - I(\tau) = \frac{1}{1 + \frac{\eta}{1-\eta} e^{\tau}}. \quad (\text{A4b})$$

The rate of new infections is then given by

$$\begin{aligned} j(\tau) &= S(\tau)I(\tau) = \frac{1}{2 + \frac{\eta}{1-\eta} e^{\tau} + \frac{1-\eta}{\eta} e^{-\tau}} \\ &= \frac{1}{2[1 + \cosh(\tau - \ln \frac{1-\eta}{\eta})]} = \frac{1}{4 \cosh^2[\frac{\tau - \ln \frac{1-\eta}{\eta}}{2}]}, \end{aligned} \quad (\text{A5})$$

to which we refer as the SI-type new infection rate in the main text.

Appendix B. Integro-Differential Equation for the SIRD Model

Here we consider the case of no vaccinations, i.e. $v = b = 0$ and $V(\tau) = 0$. In some aspects the resulting SIRD-model is simpler than the SIRVD-model, e.g. here the simpler relation $J(\tau) = 1 - S(\tau)$ holds. This facilitates the general integro-differential equations (26)–(30) derived for the more general SIRVD model. Here, Equation (25) reduces to

$$\kappa(\tau) = 1 - J(\tau) - \frac{d}{d\tau} \ln \left[\frac{j(\tau)}{1 - J(\tau)} \right], \quad (\text{A6})$$

where

$$\kappa(\tau) = k(\tau) + q(\tau). \quad (\text{A7})$$

With the initial conditions Equation (A6) integrates to

$$\frac{j(\tau)}{1 - J(\tau)} = -\frac{d}{d\tau} \ln(1 - J(\tau)) = \eta \exp \int_0^{\tau} dz [1 - J(z) - \kappa(z)], \quad (\text{A8})$$

or alternatively

$$j(\tau) = \eta e^{-\int_0^{\tau} dz \kappa(z)} \frac{d}{d\tau} e^{\tau - \int_0^{\tau} dz J(z)} = \eta [1 - J(\tau)] e^{\int_0^{\tau} dz [1 - \kappa(z) - J(z)]}. \quad (\text{A9})$$

In terms of $S(\tau) = 1 - J(\tau)$ in this case Equation (A8) reads

$$\frac{d \ln S(\tau)}{d\tau} = \frac{dS(\tau)/d\tau}{S(\tau)} = -\eta \exp \int_0^{\tau} dz [S(z) - \kappa(z)], \quad (\text{A10})$$

which with the initial condition $S(\tau = 0) = 1 - \eta$ integrates to

$$S(\tau) = (1 - \eta) \exp \left[-\eta \int_0^{\tau} dx \exp \left(\int_0^x dz [S(z) - \kappa(z)] \right) \right]. \quad (\text{A11})$$

By writing $S = e^{\ln S}$ the last equation provides

$$\ln \frac{S}{1 - \eta} = - \int_0^{\tau} dx H(x) e^{\int_0^x dz S(z)}, \quad (\text{A12})$$

with the function $H(x) = e^{\ln \eta - \int_0^x dz \kappa(z)}$. Equation (A11) is equivalent to

$$J(\tau) = 1 - (1 - \eta) \exp \left[-\eta \int_0^\tau dx \exp \left(\int_0^x dz [1 - J(z) - \kappa(z)] \right) \right], \quad (\text{A13})$$

whereas Equation (A10) can be written as

$$e^{\int_0^\tau dz \kappa(z)} \frac{dS}{d\tau} = -\eta \frac{d}{d\tau} e^{\int_0^\tau dz S(z)}. \quad (\text{A14})$$

Equation (A9) yields for Equations (15), (17)–(19) in the SIRD case

$$I(\tau) = \frac{j(\tau)}{1 - J(\tau)} = \eta e^{\int_0^\tau dz [1 - \kappa(z) - J(z)]}, \quad (\text{A15a})$$

$$R(\tau) = \eta \int_0^\tau dx k(x) e^{\int_0^x dz [1 - \kappa(z) - J(z)]}, \quad (\text{A15b})$$

$$D(\tau) = \eta \int_0^\tau dx q(x) e^{\int_0^x dz [1 - \kappa(z) - J(z)]}, \quad (\text{A15c})$$

$$d(\tau) = \frac{dD(\tau)}{d\tau} = q(\tau)I(\tau) = \eta q(\tau) e^{\int_0^\tau dz [1 - \kappa(z) - J(z)]}, \quad (\text{A15d})$$

respectively. Equations (A8)–(A10) represent the exact solutions for the SIRD and SIR equations for $\kappa = k(\tau) + q(\tau) = k_{\text{tot}}$. The only difference between these two occurs for the calculation of the fractions of recovered and removed persons. The integral equation (A12) cannot be solved analytically for $S(\tau)$ in general, but for $\eta \ll 1$ we show in Section 4 that an analytic solution exists within a range of k_{tot} values.

Appendix C. Solution of Wright's Transcendental Equation

With $z = -b_0 \tau_d$ Equation (176) is equivalent with Wright's [29] transcendental equation

$$(q + pz)e^z = rz + s, \quad (\text{A16})$$

with $q = q_0 > 0$, $p = q_1 G / b_0 > 0$, $r = q_1 G [k_0 + 2q_0 + G] / b_0 > 0$ and $s = q_0(k_0 + q_0) + q_1 G > 0$ and we follow Wright's arguments, while he focused on the roots of Equation (A16). Because $pr \neq 0$ we substitute

$$z = Z - \ln(p/r) = Z + \ln(k_0 + 2q_0 + G), \quad (\text{A17})$$

providing for Equation (A16)

$$(Z - a + b)e^Z = Z - a - b \quad (\text{A18})$$

with the real-valued constants

$$a = -\frac{1}{2} \left(\frac{s}{r} + \frac{q}{p} \right) + \ln \left(\frac{p}{r} \right) = -\ln(k_0 + 2q_0 + G) - \frac{b_0 q_0}{q_1 G} + b, \quad (\text{A19a})$$

$$b = -\frac{1}{2} \left(\frac{s}{r} - \frac{q}{p} \right) = \frac{b_0 q_0 q_0 + (1 - q_1 / q_0) G}{q_1 G 2(k_0 + 2q_0 + G)}. \quad (\text{A19b})$$

This confirms Equation (180). Note that for $a = b = 0$ the Equation (A18) is solved by $Z = 0$. To arrive at Equations (A16) and (A19a) we assumed $G\tau_d \ll 1$. While $b > 0$, for sufficiently small G/b_0 the a is negative, more precisely, as soon as

$$\frac{G}{b_0} < -\frac{q_0}{q_1} \frac{1 - q_0 / [2(k_0 + 2q_0 + G)]}{\ln(k_0 + 2q_0 + G)}. \quad (\text{A20})$$

Because a can be assumed negative, we introduce the positively valued

$$A = b - a = \frac{q}{p} - \ln\left(\frac{p}{r}\right) = \ln(k_0 + 2q_0 + G) + \frac{b_0q_0}{q_1G}, \quad (\text{A21})$$

so that $a = -(A - b)$. Equation (A18) then becomes

$$e^Z = 1 - \frac{2b}{Z + A}. \quad (\text{A22})$$

It is evident that Equation (A22) has no solutions for positive values of $Z > 0$, as its left-hand side is always larger than unity in that case while the right-hand side is smaller than unity. For negative values of $Z = -X$ with $X > 0$ Equation (A22) reads

$$e^{-X} = 1 - \frac{2b}{A - X}, \quad (\text{A23})$$

and the substitution $X = Ay$ in Equation (A23) yields

$$e^{-Ay} = 1 - \frac{2b}{A(1 - y)}, \quad (\text{A24})$$

which only has solutions for $y < 1$ because b is positive. Equation (A24) will be used below to derive approximants X_0 and X_1 , while approximant X_2 considers Equation (A18) as the starting point. In deriving the approximants it will turn out important to recall that a fulfills the inequality $a < a_{\max} \leq 0$ with a_{\max} given by Equation (181). We can thus write $a = a_{\max} - \zeta$ with semipositive ζ . An important limiting feature is $\lim_{b \rightarrow 0} a_{\max} = 0$.

Appendix C.1. Derivation of X_0

Expanding $e^{-Ay} \simeq 1 - Ay$, which requires $y \leq A^{-1}$ (or $X \leq 1$) we obtain from Equation (A24)

$$y(y - 1) \simeq -\frac{2b}{A^2}, \quad (\text{A25})$$

with the two solutions

$$y_1 = \frac{1 - \sqrt{1 - 8b/A^2}}{2} \simeq \frac{2b}{A^2}, \quad (\text{A26a})$$

$$y_2 = \frac{1 + \sqrt{1 - 8b/A^2}}{2} \simeq 1 - \frac{2b}{A^2}. \quad (\text{A26b})$$

Because $2b/A^2 \ll 1$, since

$$\frac{2b}{A^2} \leq \frac{2b}{(b - a_{\max})^2} \leq \lim_{b \rightarrow 0} \frac{2b}{(b - a_{\max})^2} = \lim_{b \rightarrow 0} \left(\frac{1}{4} - \frac{\sqrt{b}}{4\sqrt{2}} \right) = \frac{1}{4}, \quad (\text{A27})$$

only the solution y_1 fulfils the requirement $y_1 \leq A^{-1}$, corresponding to $(2b/A) \leq 1$ which is a valid inequality, as

$$\frac{2b}{A} = \frac{2b}{b - a} \leq \frac{2b}{b - a_{\max}} = \frac{2b}{b + \sqrt{b(2 + b) + \cosh^{-1}(1 + b)}} \leq 1. \quad (\text{A28})$$

The inequality (A27) therefore also implies that the argument under the square root is positive, $1 - 8b/A^2 > 0$. With $X_0 = Ay_1 < 1$ and $A = b - a$ this completes the derivation of X_0 in Equation (182a).

Appendix C.2. Derivation of X_2

Because $y < 1$, here we assume $y \ll 1$ and use the approximation $(1 - y)^{-1} \simeq 1 + y$ in Equation (A24) to obtain

$$e^{-Ay} \simeq -\frac{2b}{A} \left(y + 1 - \frac{A}{2b} \right), \quad (\text{A29})$$

with the solution

$$y = \frac{A}{2b} - 1 + \frac{1}{A} W_{-1} \left(-\frac{A^2}{2be^{A(\frac{A}{2b}-1)}} \right), \quad (\text{A30})$$

where W_{-1} is the non-principal branch of Lambert's W function. For $a < a_{\max}$ stated in Equation (181), the argument of the Lambert function is negative, decreases with increasing b , and resides within the interval $[-1/e, 0]$ so that W_{-1} is real-valued and $W_{-1} < -1$ holds. The principal branch W_0 of Lambert's function solves Equation (A29) as well, but can be ruled out by considering the limit $b \rightarrow 0$ and $a \rightarrow a_{\max}$. In this limit the argument of Lambert's function evaluates, with $A = b - a$, to

$$\lim_{b \rightarrow 0} -\frac{(b - a_{\max})^2}{2be^{(b-a_{\max})(\frac{b-a_{\max}}{2b}-1)}} = -\frac{4}{e^4}. \quad (\text{A31})$$

On the other hand

$$\lim_{b \rightarrow 0} \frac{(b - a_{\max})^2}{2b} - b + a_{\max} = 4. \quad (\text{A32})$$

For the argument stated in Equation (A31), Lambert's functions evaluate to $W_0(-4/e^4) \approx -0.079$ and $W_{-1}(-4/e^4) = -4$, respectively. Since we know that $X = Ay = 0$ solves Equation (A23) in the same limit, the principal branch W_0 can be ruled out. With $X_2 = Ay \ll A$ this completes the derivation of X_2 in Equation (182c).

Appendix C.3. Derivation of X_1

Equation (A18), technically divided by $e^Z - 1$, can also be written as

$$a = Z + b \coth \left(\frac{Z}{2} \right). \quad (\text{A33})$$

Here we depart from Wright's arguments and solve Equation (A33) with asymptotic expansions of the coth-function. For values of $|Z| \leq 2$ we approximate $\coth(Z/2) \simeq 2/Z[1 + (Z^2/12)]$, so that in this range Equation (A33) reduces to the quadratic

$$\left(1 + \frac{b}{6} \right) Z^2 - aZ + 2b = 0, \quad (\text{A34})$$

with the two solutions

$$Z_{\pm} = \frac{3a \pm \sqrt{9a^2 - 12b(6+b)}}{6+b}. \quad (\text{A35})$$

The term under the square root is not strictly semipositive for any $a < a_{\max}$, but Z_{\pm} is real-valued for $a < -2\sqrt{b(6+b)}/3$, which is only slightly below a_{\max} ; for $b < 10$ it is only 3% below a_{\max} , giving rise to the tiny white region in top right corner of Figure A1. For this reason the question about the suitable sign in Equation (A35) cannot be answered by considering the limit $b \rightarrow 0$ and $a \rightarrow a_{\max}$, as before. Instead, consider the following: Inserting $a = Z + \chi \sinh(Z)$ and $b = \chi[\cosh(Z) - 1]$ solves Equation (A33) for any choice of χ , i.e., one can write

$$a = Z - \sqrt{b(b+2\chi)}, \quad Z = -\cosh^{-1} \left(\frac{b+\chi}{\chi} \right), \quad (\text{A36})$$

for positive χ . Using $\chi = 1$ we had derived a_{\max} . Using $\chi = 0$ in Equation (A36) yields $b = 0$ and $a = Z$, while the 2nd relation in Equation (A36) in this limit is just the identity $Z = Z$. Inserting this special case of $a = Z$ and $b = 0$ into Equation (A35) yields $Z_{\pm} = (Z \pm Z)/2$. As we expect to find $Z_{\pm} = Z$, the suitable solution is Z_+ . With $X_1 = -Z_+ < 2$ this completes the derivation of X_1 in Equation (182b).

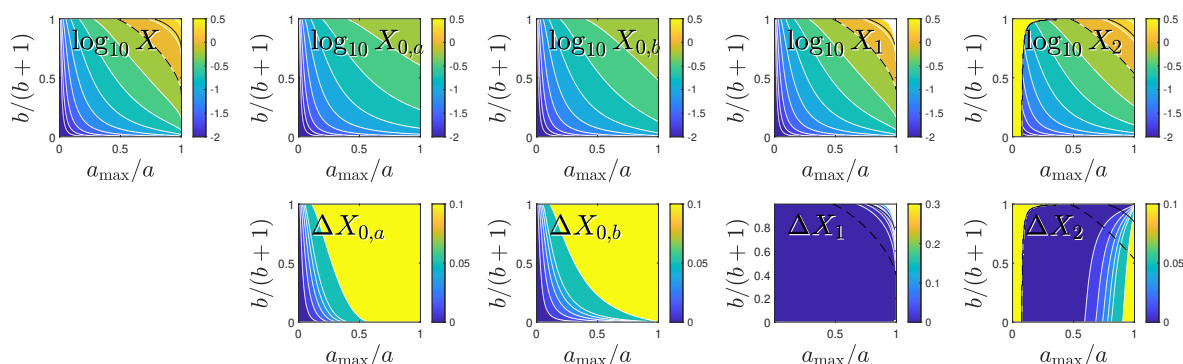


Figure A1. Top row from left to right: The exact solution X to Equation (178) or (179) versus a_{\max}/a and $b/(b+1)$ with the negative a_{\max} defined by Equation (181), approximants $X_{0,a}$, $X_{0,b}$, X_1 , and X_2 given by Equation (182). For any X and b , the exact solution corresponds to $a = -X - b \coth(X/2)$ according to Equation (179). Two contourlines are highlighted in each panel, if they exist: $X = 1$ (dashed black) and $X = 2$ (solid black). In the X_1 panel, the X_1 is undefined in the small white region in the top right corner, defined by $a < -2\sqrt{b(6+b)}/3$. In the X_2 panel, the X_2 cannot be evaluated numerically in the yellow region which is characterized by $X > 1$ and $a > a_{\max}/2$. Bottom row from left to right: The relative deviation ΔX between approximants $X_{0,a}$, $X_{0,b}$, X_1 and X_2 and the exact numerical solution X , again versus a_{\max}/a and $b/(b+1)$. The color scale ranges from blue (relative deviation below 1%, to yellow (relative deviation above 10%). Approximant X_1 performs very well except in the tiny top right corner (large b , a close to a_{\max}), where X_2 has some advantage.

References

1. Bailey, N.T. *The Mathematical Theory of Infectious Diseases and its Applications*; Charles Griffin & Company Ltd., Bucks, United States, 1975.
2. Hethcote, H.W. The mathematics of infectious diseases. *SIAM Rev.* **2000**, *42*, 599–653.
3. Estrada, E. Covid-19 and Sars-Cov-2, Modeling the present, looking at the future. *Phys. Rep.* **2020**, *869*, 1. <https://doi.org/10.1016/j.physrep.2020.07.005>.
4. Kermack, W.O.; McKendrick, A.G. A contribution to the mathematical theory of epidemics. *Proc. R. Soc. A* **1927**, *115*, 700. <https://doi.org/10.1098/rspa.1927.0118>.
5. Kendall, D.G. Deterministic and stochastic epidemics in closed populations. In Proceedings of the Proceedings of the Third Berkeley Symposium on Mathematical Statistics and Probability. University of California Press: Berkeley, CA, USA, 1956, Vol. 4, p. 149. <https://doi.org/10.1525/9780520350717-011>.
6. Schlickeiser, R.; Kröger, M. Analytical solution of the SIR-model for the temporal evolution of epidemics: Part B. Semi-time case. *J. Phys. A* **2021**, *54*, 175601. <https://doi.org/10.1088/1751-8121/abed66>.
7. Albidah, A.B. A proposed analytical and numerical treatment for the nonlinear SIR model via a hybrid approach. *Mathematics* **2023**, *11*, 2749. <https://doi.org/10.3390/math1122749>.
8. Schlickeiser, R.; Kröger, M. Analytical modeling of the temporal evolution of epidemics outbreaks accounting for vaccinations. *Physics* **2021**, *3*, 386–426. <https://doi.org/10.3390/physics3020028>.
9. Babaei, N.A.; Özer, T. On exact integrability of a COVID-19 model: SIRV. *Math. Meth. Appl. Sci.* **2023**, *1*, 1–18. <https://doi.org/10.1002/mma.8874>.
10. Rifhat, R.; Teng, Z.; Wang, C. Extinction and persistence of a stochastic SIRV epidemic model with nonlinear incidence rate. *Adv. Diff. Eqs.* **2021**, *2021*, 200. <https://doi.org/10.1186/s13662-021-03347-3>.
11. Ameen, I.; Baleanu, D.; Ali, H.M. An efficient algorithm for solving the fractional optimal control of SIRV epidemic model with a combination of vaccination and treatment. *Chaos Solit. Fract.* **2020**, *137*, 109892. <https://doi.org/10.1016/j.chaos.2020.109892>.

12. Oke, M.; Ogunmiloro, O.M.; Akinwumi, C.T.; Raji, R.A. Mathematical Modeling and Stability Analysis of a SIRV Epidemic Model with Non-linear Force of Infection and Treatment. *Commun. Math. Appl.* **2019**, *10*, 717–731. <https://doi.org/10.26713/cma.v10i4.1172>.
13. Marinov, T.T.; Marinova, R.S. Adaptive SIR model with vaccination: simultaneous identification of rates and functions illustrated with COVID-19. *Sci. Rep.* **2022**, *12*, 15688. <https://doi.org/10.1038/s41598-022-20276-7>.
14. Haas, F.; Kröger, M.; Schlickeiser, R. Multi-Hamiltonian structure of the epidemics model accounting for vaccinations and a suitable test for the accuracy of its numerical solvers. *J. Phys. A* **2022**, *55*, 225206. <https://doi.org/10.1088/1751-8121/ac6995>.
15. Li, X.; Li, X.; Zhang, Q. Time to extinction and stationary distribution of a stochastic susceptible-infected-recovered-susceptible model with vaccination under Markov switching. *Math. Popul. Stud.* **2020**, *27*, 259–274. <https://doi.org/10.1080/08898480.2019.1626633>.
16. Cai, C.R.; Wu, Z.X.; Guan, J.Y. Behavior of susceptible-vaccinated-infected-recovered epidemics with diversity in the infection rate of individuals. *Phys. Rev. E* **2013**, *88*, 062805. <https://doi.org/10.1103/PhysRevE.88.062805>.
17. Wang, J.; Zhang, R.; Kuniya, T. A reaction-diffusion Susceptible-Vaccinated-Infected-Recovered model in a spatially heterogeneous environment with Dirichlet boundary condition. *Math. Comp. Simul.* **2021**, *190*, 848–865. <https://doi.org/10.1016/j.matcom.2021.06.020>.
18. Khader, M.M.; Adel, M. Numerical Treatment of the Fractional Modeling on Susceptible-Infected-Recovered Equations with a Constant Vaccination Rate by Using GEM. *Int. J. Nonlin. Sci. Numer. Simul.* **2019**, *20*, 69–75. <https://doi.org/10.1515/ijnsns-2018-0187>.
19. Dai, Y.; Zhou, B.; Jiang, D.; Hayat, T. Stationary distribution and density function analysis of stochastic susceptible-vaccinated-infected-recovered (SVIR) epidemic model with vaccination of newborns. *Math. Meth. Appl. Sci.* **2022**, *45*, 3401–3416. <https://doi.org/10.1002/mma.7986>.
20. Schlickeiser, R.; Kröger, M. Analytical solution of the SIR-model for the not too late temporal evolution of epidemics for general time-dependent recovery and infection rates. *Covid* **2023**, *3*, 1781–1796. <https://doi.org/10.3390/covid3120123>.
21. Kröger, M.; Schlickeiser, R. On the analytical solution of the SIRV-model for the temporal evolution of epidemics for general time-dependent recovery, infection and vaccination rates. *Mathematics* **2024**, *12*, 326. <https://doi.org/10.3390/math12020326>.
22. Schlickeiser, R.; Kröger, M. Forecast of omicron wave time evolution. *Covid* **2022**, *2*, 216–229. <https://doi.org/10.3390/covid2030017>.
23. Khalsaraei, M.M.; Shokri, A.; Ramos, H.; Yao, S.W.; Molayi, M. Efficient Numerical Solutions to a SIR Epidemic Model. *Mathematics* **2022**, *10*. <https://doi.org/10.3390/math10183299>.
24. Khalsaraei, M.M.; Shokri, A.; Noeiaghdam, S.; Molayi, M. Nonstandard Finite Difference Schemes for an SIR Epidemic Model. *Mathematics* **2021**, *9*. <https://doi.org/10.3390/math9233082>.
25. Shampine, L.F.; Gordon, M.K. *Computer Solution of Ordinary Differential Equations: the Initial Value Problem*; W. H. Freeman, San Francisco, 1975.
26. Schlickeiser, R.; Kröger, M. Determination of a key pandemic parameter of the SIR-epidemic model from past Covid-19 mutant waves and its variation for the validity of the Gaussian evolution. *Physics* **2023**, *5*, 205–214. <https://doi.org/10.3390/physics5010016>.
27. Hazewinkel, M., Ed. *Galois theory*; European Mathematical Society Press, Berlin, 2001.
28. Kröger, M.; Schlickeiser, R. Analytical solution of the SIR-model for the temporal evolution of epidemics. Part A: Time-independent reproduction factor. *J. Phys. A* **2020**, *53*, 505601. <https://doi.org/10.1088/1751-8121/abc65d>.
29. Wright, E.M. Stability criteria and the real roots of a transcendental equation. *J. Soc. Indust. Appl. Math.* **1961**, *9*, 136–148.
30. Secer, A.; Ozdemir, N.; Bayram, M. A Hermite Polynomial Approach for Solving the SIR Model of Epidemics. *Mathematics* **2018**, *6*. <https://doi.org/10.3390/math6120305>.

Disclaimer/Publisher's Note: The statements, opinions and data contained in all publications are solely those of the individual author(s) and contributor(s) and not of MDPI and/or the editor(s). MDPI and/or the editor(s) disclaim responsibility for any injury to people or property resulting from any ideas, methods, instructions or products referred to in the content.